



Anatomy of the sense of touch in sea otters: Cutaneous mechanoreceptors and structural features of glabrous skin

Sarah McKay Strobel¹  | Melissa A. Miller² | Michael J. Murray³ | Colleen Reichmuth⁴ 

¹Department of Ecology and Evolutionary Biology, University of California Santa Cruz, Santa Cruz, California, USA

²California Department of Fish and Wildlife, Marine Wildlife Veterinary Care and Research Center, Santa Cruz, California, USA

³Monterey Bay Aquarium, Monterey, California, USA

⁴Long Marine Laboratory, Institute of Marine Sciences, Santa Cruz, California, USA

Correspondence

Sarah McKay Strobel, Department of Ecology and Evolutionary Biology, University of California Santa Cruz, 115 McAllister Way, Santa Cruz, CA 95060.

Email: smstrobel@ucsc.edu, smstrobel@gmail.com

Funding information

Department of Education Graduate Assistance in Areas of National Need Fellowship, Grant/Award Number: P200A150100; Sea Otter Foundation and Trust

Abstract

Sea otters (*Enhydra lutris*) demonstrate rapid, accurate tactile abilities using their paws and facial vibrissae. Anatomical investigations of neural organization in the vibrissal bed and somatosensory cortex coincide with measured sensitivity, but no studies describe sensory receptors in the paws or other regions of glabrous (i.e., hairless) skin. In this study, we use histology to assess the presence, density, and distribution of mechanoreceptors in the glabrous skin of sea otters: paws, rhinarium, lips, and flipper digits, and we use scanning electron microscopy to describe skin-surface texture and its potential effect on the transduction of mechanical stimuli. Our results confirm the presence of Merkel cells and Pacinian corpuscles, but not Meissner corpuscles, in all sea otter glabrous skin. The paws showed the highest density of Merkel cells and Pacinian corpuscles. Within the paw, relative densities of mechanoreceptor types were highest in the distal metacarpal pad and digits, which suggests that the distal paw is a tactile fovea for sea otters. In addition to the highest receptor density, the paw displayed the thickest epidermis. Rete ridges (epidermal projections into the dermis) and dermal papillae (dermal projections into the epidermis) were developed across all glabrous skin. These quantitative and qualitative descriptions of neural organization and physical features, combined with previous behavioral results, contribute to our understanding of how structure relates to function in the tactile modality. Our findings coincide with behavioral observations of sea otters, which use touch to maintain thermoregulatory integrity of their fur, explore objects, and capture visually cryptic prey.

KEYWORDS

Enhydra lutris, integument, mechanoreceptor distribution, Merkel cell, Pacinian corpuscle

1 | INTRODUCTION

Although hair is a shared characteristic of all mammals, glabrous skin can be essential for tactile feedback during locomotion, foraging, predator avoidance, intraspecific communication, and exploration, as well as for physiological processes, such as thermoregulation and

osmoregulation. Consistent with patterns in other sensory modalities, the structure and distribution of neural tissue and sensory receptors in glabrous skin influences sensory perception, and differences within and across species can provide a deeper understanding of behavior and ecological pressures. Sea otters (*Enhydra lutris*) provide an interesting case to examine the links between

structure and function for the sense of touch, due to their visually cryptic prey resources, high energetic requirements, and high thermoregulatory demands from constant heat loss to the aquatic environment. As shallow divers distributed along the eastern Pacific coastline of North America, sea otters forage under water for visually cryptic, sessile, hard-shelled benthic invertebrates. Relative to other diving predators, unsuccessful foraging is especially costly for sea otters, since they have one of the highest mass-specific metabolic rates among mammals (Costa & Kooyman, 1982), as well as spatial separation between underwater prey capture at depth and prey consumption at the water's surface (e.g., Bodkin, Esslinger, & Monson, 2004; Kenyon, 1969).

Sea otters have highly dense fur that provides an effective insulative barrier between skin and seawater at the water's surface and while foraging (Kuhn, Ansorge, Godynicki, & Meyer, 2010; Williams, Allen, Groff, & Glass, 1992). Even so, sea otters have retained regions of glabrous skin, including the rhinarium, lips, ears, and volar surfaces of the forefeet (i.e., paws) and the hindfeet (i.e., flippers). The surface area of glabrous skin in sea otters relative to terrestrial mustelids is hypertrophied for the paws but reduced for the flippers. The elongated webbed flippers are covered in fur, except at the distal ends, where a single ventral volar pad and a non-retractable dorsal claw occur for each toe (Figure 1d; Kenyon, 1969; Pocock, 1928). In contrast, the entire

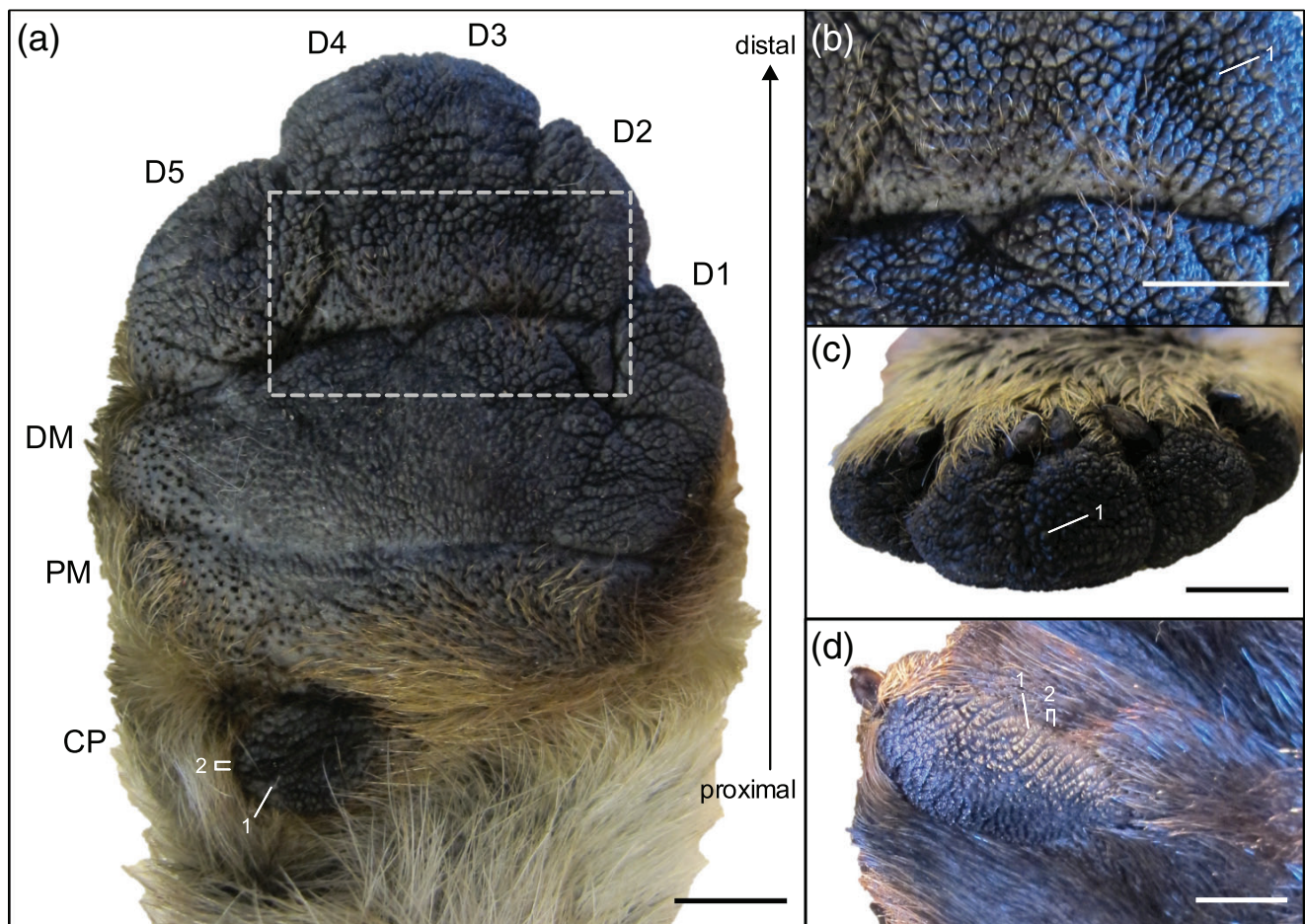


FIGURE 1 (a–c) Palmar view of the sea otter right paw (forefoot) and (d) plantar view of the sea otter third digit pad of the right flipper (hindfoot); scale bars = 1 cm. (a) The paw comprises a fused palmar surface with eight regions of interest (ROIs) delineated by creating: ulnar carpal pad (CP), proximal metacarpal pad (PM), distal metacarpal pad (DM), and five digits (D1–D5). Hair and follicles are distributed across the proximal metacarpal pad and in the digit–palmar interface, represented by the boxed area in (a) and the corresponding higher magnification image in (b). (c) Glabrous skin extends over the digit tips to the base of the semi-retractable claws. Note that the pads of digits 3 and 4 are delineated clearly at the distal tip of the paw, but not on the palmar surface (a). In contrast, a thin margin of hair separates the base of the claw from the digit pad in the flipper pad (d). The surface texture of the paw pad represented in (a–c) varies along the proximodistal axis and from that in the digit pad of the flipper (d). In the metacarpal and digit pads of the paw, skin surface comprised round protrusions (1) that were not arranged in a ridged pattern (b,c); the protrusions increased in density and height from the proximal to distal portions of the paw pad (a,b). In contrast, round protrusions (1) were aligned in transverse ridges (2) in both the carpal and flipper digit pads (a,d). Differences in skin pigmentation (a–d) are artifacts due to variable lighting when photographs were taken

palmar surface of each paw is fused, with creased delineations between five digit pads (somewhat reduced between the third and fourth digits), two metacarpal pads, and an ulnar carpal pad (Figure 1a–c; Pocock, 1928). Sea otters can move their digits independently even within the fused palmar pads, and they clearly use their paws to groom their fur, dexterously open hard-shelled prey, manipulate tools, and explore objects in their environment (S.M. Strobel, personal observation). The claws on sea otter paws are semi-retractable; they are reduced relative to terrestrial carnivores (Figure 1c; Kenyon, 1969), in a similar pattern as other amphibious tactile-oriented mammals (Hamrick, 2001). They tend to keep their claws relaxed during object exploration and extend them primarily during object manipulation (S.M. Strobel, personal observation). Behavioral measurements of paw tactile sensitivity in a trained sea otter (Strobel, Sills, Tinker, & Reichmuth, 2018) support the long-held presumption that touch is specialized in these coastal, amphibious mammals (see, e.g., Kenyon, 1969; Radinsky, 1968; Riedman & Estes, 1990) and suggest the retention and enhancement of glabrous paw skin has served an important function in sea otter evolutionary history.

Although sea otter paws show adaptations for enhanced touch abilities, sensitivity and corresponding function may differ across the palmar paw, since a sea otter preferentially used the distal palmar paw (digits and distal metacarpal pad) to make discrete, rapid touch explorations of texture (Strobel et al., 2018). In addition, the extent to which the glabrous rhinarium and lips contribute to measured whisker sensitivity has not been explicitly tested. As the first point of contact between an animal and an approaching stimulus, facial skin—including the rhinarium, lips, and eyelids—can show high innervation and abundant sensory receptors in terrestrial mammals (Abrahams, Hodgins, & Downey, 1987; Halata, 1990; Halata & Munger, 1983; Montagna, Roman, & Macpherson, 1975; Munger & Halata, 1983), even in species with sensitive whisker-based touch (Halata, 1990; Silverman, Munger, & Halata, 1986). Although sea otters show differential use of their glabrous skin regions, and the surface anatomies of these regions vary substantially, no studies have examined the underlying sensory architecture in their glabrous skin and its influence on touch ability.

As cutaneous sensory structures that range from free nerve endings to highly specialized encapsulated neurons, mechanoreceptors mediate a wide variety of tactile sensations and can be categorized based on their specialized or generalized response to different types and intensities of mechanical stimuli. Merkel cells are slowly adapting type I receptors that have high spatial resolution

and detect subtle skin deformations resulting from sustained light touch, such as points, edges, and curvature (Iggo & Muir, 1969; Johnson, 2001). Meissner corpuscles are rapidly adapting touch receptors with poor spatial resolution but high sensitivity for low-frequency vibration and motion perception, which are essential for grip control of objects (Johnson, 2001). Pacinian corpuscles are rapidly adapting pressure receptors with poor spatial resolution but extreme sensitivity to high-frequency vibrations, which is essential for indirectly perceiving vibrations transmitted through a tool to the skin (Bell, Bolanowski, & Holmes, 1994; Johnson, 2001). Mechanoreceptor types are differentially distributed across the body's skin, and variation in density of each type corresponds with variation in tactile perception (Andres & v Düring, 1990; Johansson & Vallbo, 1979; Paré, Smith, & Rice, 2002). In addition to mechanoreceptor density, skin-surface texture and the topography of the epidermal-dermal interface may influence tactile perception by mediating grip strength, transduction of mechanical stimuli, and mechanical properties of the skin (Cartmill, 1979; Cauna, 1985; Halata, 1990; Hamrick, 2001). Properties of the external environment can also directly or indirectly affect mechanoreceptor function. Cold ambient temperatures lead to reduced tactile sensitivity in humans (Bolanowski & Verrillo, 1982; Gescheider, Thorpe, Goodarz, & Bolanowski, 1997; Verrillo & Bolanowski, 1986), which may result from negative effects of temperature on action potentials, signal amplification or transmission, or localized blood flow.

The current study complements behavioral work by the same researchers (Strobel et al., 2018) to determine how form supports function and, ultimately, contributes to sea otter foraging behavior. We used histology and scanning electron microscopy to assess structural and neural features of the peripheral touch system across four glabrous skin regions in sea otters—rhinarium, lips, and palmar surfaces of the paws and flippers—with tissues obtained from postmortem animals. Since a baseline mechanoreceptor density in sea otter skin is unknown, and the rhinarium and lips can be close to objects during exploration and to prey during search and capture behavior, we examined all glabrous skin regions to provide an objective, within-animal comparison and reveal which regions and subregions are most likely to have high spatial resolution or sensitivity in sea otters. We first determined which mammalian cutaneous mechanoreceptors are present in sea otters, including an assessment of Merkel cells, Meissner corpuscles, and Pacinian corpuscles. After identification and abundance counts for each mechanoreceptor type in glabrous skin regions, we compared morphology and regional variation in density to

those described for other terrestrial and amphibious mammals and previously measured touch ability. Based on our findings from this and prior studies, we speculated on the function of skin texture and thickness for sensitivity and robustness and the thermoregulatory implications of increased neural and circulatory investment. Our findings contribute to the fields of sensory biology and foraging ecology by broadening current understanding of how tactile perception mediates predator–prey interactions in an aquatic environment.

2 | MATERIALS AND METHODS

2.1 | Subjects and tissue collection

We obtained tissues from three adult sea otters (two males, one female) that were humanely euthanized due to serious injuries sustained prior to stranding. Tissue collection occurred within 20 min of death. For each sea otter, we excised the rhinarium, the lips, the left and right paws at the radiocarpal joint, and the left and right second or third flipper digit at the metatarsophalangeal joint and placed them in sealed containers on ice. Within 3 hr, we removed the integumentary tissue from each region, including the epidermis, dermis, and hypodermis located superficial to the flexor tendons. In addition to treating the rhinarium, lips, and flipper plantar pad as three regions of interest (ROIs), we further segmented the integumentary tissue from the palmar pad of each paw into eight ROIs: five digit pads, two metacarpal pads, and the ulnar carpal pad, using natural creases in the pad to guide sampling efforts (Figure 1a). We immersed each ROI in 10% neutral buffered formalin.

2.2 | Tissue preparation and imaging

Within 2 months of fixation, we trimmed one to two representative tissues from each ROI along the sagittal plane to fit into standard histology cassettes (3 cm × 2.5 cm). At the Veterinary Histology Lab at the University of California Davis, tissues were paraffin embedded and 5- μ m-thick sagittal slices were obtained using a rotary microtome. The tissue sections (one to two from each sample site) were mounted on glass slides and stained with hematoxylin and eosin (H&E) according to standard protocols. We obtained two-dimensional images for each H&E-stained tissue at $\times 10$ magnification using a Zeiss AxioImager Z2 widefield microscope equipped with a Zeiss AxioCam 506 color camera (Carl Zeiss Microscopy GmbH, Jena, Germany). We stitched the resulting 100+ tiles using Zeiss Zen Pro software to form a single

composite image for each H&E-stained tissue. The composite image was stored as a .czi file to retain tissue scaling and metadata.

Additional 1 × 1 × 1 cm sections from the rhinarium, lips, third digit pad from the right paw, and third digit pad from the right flipper of one sea otter were prepared for imaging via scanning electron microscopy. We washed the samples in 1× phosphate-buffered saline (PBS), dehydrated them in a graded ethanol series (30, 50, 70, 80, 90, 95, and 100%), and then transferred the dehydrated samples from 100% ethanol into a critical point dryer to replace the ethanol with supercritical-fluid carbon dioxide. Following critical point drying, the samples were mounted onto stubs, sputter-coated with gold, and tile-imaged at 25× or 40× magnification in a Quanta 3D field emission scanning electron microscope (Field Electron and Ion Company, Hillsboro, OR). We stitched the resulting tiles to form a single composite image per sample.

2.3 | Measurement of tissue area and epidermal layer thickness

To determine the surface area for each H&E-stained tissue we used custom macro and manual tracing in Fiji (Schindelin et al., 2012). We first converted the composite image of the tissue to a gray scale 8-bit image, then used thresholding to assign each pixel into the binary categories of “tissue” or “background.” We visually compared the thresholded image to the full-color image to manually adjust our pixel cutoff value. To exclude small pieces of low-quality tissue, we manually traced a contour area around the tissue and summed the area of all traced particles larger than 100 mm. Small holes or tears were present in many tissues as a result of histological processing or natural skin morphology (e.g., the nostril in the rhinarium). To avoid overestimating surface area for these tissues, we reversed the assignment of “tissue” and “background” in the thresholded image, used the same manually traced contour area around the tissue, and summed the area of all traced particles smaller than 0.2 mm. We continued to visually compare the thresholded image to the full-color image and adjusted the upper size limit of traced particles as needed to more accurately reflect the maximum size of artifactual gaps in the tissue. We subtracted the summed area of artifactual gaps from the summed tissue area to calculate total surface area occupied by epidermis, dermis, hypodermis, and associated dermal structures, such as nerves and blood vessels.

In addition to total surface area, we calculated surface area for tissue considered biologically relevant for each

mechanoreceptor type. Since Merkel cells only occur in the stratum basale of the epidermis, we considered the stratum basale as the biologically relevant tissue. We manually traced a contour line in Fiji along the stratum basale-dermis juncture for each tissue to calculate its curvilinear length (mm) and report density of histologically apparent Merkel cells (mean cells/mm \pm SD). Since Meissner corpuscles and Pacinian corpuscles do not occur in the epidermis, we considered the dermis as the biologically relevant tissue. To calculate dermal surface area (mm²), we subtracted epidermal area from total tissue area since the epidermis had a greater staining intensity and higher contrast difference from the slide background than the dermis. To calculate the epidermal area (mm²) to subtract from the total tissue area, we followed the same thresholding method described for the total surface area but assigned the epidermis as “tissue” and the rest of the tissue as “background.” We reported density of histologically apparent Pacinian corpuscles (mean corpuscles/mm² \pm SD).

A single observer was trained to identify sensory and neural structures and delineate epidermal layers (i.e., stratum corneum, stratum lucidum, stratum granulosum, stratum spinosum, and stratum basale; Figure 4b) within sea otter skin. The observer used the straight line tracing tool in Zen Pro to measure the thickness of each epidermal layer perpendicular to the stratum basale at 12 different points approximately equidistant for each tissue. We calculated total epidermal thickness at each measurement point as the sum of the epidermal layers' thicknesses. To assess how epidermal layer thickness varied across ROIs, we divided epidermal layer thickness by total epidermal thickness to calculate proportional thickness for each epidermal layer. For each ROI and otter, we report mean total epidermal thickness and epidermal layer thickness, as well as mean proportional thickness for each epidermal layer.

2.4 | Mechanoreceptor morphology and distribution

The observer scanned each tiled image for each tissue to census three mechanoreceptor types that were reliably identifiable based on morphology and staining patterns (Bell et al., 1994; Halata, 1990; Merkel, 1875; Young, O'Dowd, & Woodford, 2014): Merkel cells, Meissner corpuscles, and Pacinian corpuscles. However, we were unable to find any structures resembling typical Meissner corpuscles, so our methodology applies only to Merkel cells and Pacinian corpuscles. Key images were reviewed jointly by the observer and experienced veterinary

pathologists to confirm identification of structures and ensure interpretation of the histological features. Mechanoreceptor cell types were categorized with a high level of certainty and discrimination; any structures that were neural tissue but could not be confidently classified as mechanoreceptor types were categorized separately as “neural structures.”

We report the size of mechanoreceptors as area (mean \pm SD) for a subset of total Merkel cells ($n = 967$, 38.0% of total), as well as area (mean \pm SD) and maximum length (mean \pm SD) for a subset of total Pacinian corpuscles ($n = 121$, 30.2% of total). We calculated area using the polygon tracing and oval tools in Zen Pro to trace the outline of the external capsule for each mechanoreceptor type. We calculated maximum length using the straight line tracing tool in Zen Pro to trace the longest axis of the Pacinian corpuscle.

In addition to mechanoreceptor type, we assessed whether each mechanoreceptor occurred alone or within a spatial cluster of the same type (≥ 2 mechanoreceptors). For mechanoreceptors that appeared to cluster spatially, we report the number of each mechanoreceptor associated within the cluster (mean \pm SD). We also examined spatial associations between each mechanoreceptor and rete ridges (formerly, rete pegs: epidermal projections into the dermis) or dermal papillae (dermal projections into the epidermis). We noted the proximodistal orientation of each tissue from the paw digits and virtually segmented it into quadrants (distal, distal-medial, proximal-medial, and proximal) to link the position of each mechanoreceptor to its position along the proximodistal axis in a living sea otter.

2.5 | Statistical analyses

We assessed if density of each mechanoreceptor type varied across glabrous skin regions, within glabrous skin regions, between left and right sides of the body, and along the proximodistal axis of the digits using generalized linear mixed models (GLMM) and post hoc custom contrasts. We also assessed if total thickness of the epidermis and five epidermal layers varied across glabrous skin regions, within the paw pad ROIs, and between left and right sides of the body. We used R (R Core Team, Vienna, Austria) and the package lme4 (Bates, Maechler, Bolker, & Walker, 2015) to perform GLMM analyses that included either glabrous skin region, ROI, body side, or proximodistal location as the categorical fixed effect and individual sea otter as the random effect. For all models, we included a fixed intercept but random regression coefficients for the fixed effect within individual sea otter as a

random effect. For the side and proximodistal models assessed within the paw we nested ROI within individual sea otter as the random effect, and for the proximodistal model assessed within the flipper digit pads we nested slice within sea otter as the random effect to account for our multiple sampling of each ROI.

For each mechanoreceptor type, we used presence and proportional density as binomial-distributed response variables and density as a Gamma-distributed response variable. For each epidermal layer thickness and the total epidermis thickness, we used thickness as a Gamma-distributed response variable; for each epidermal layer, we used proportional thickness as a binomial-distributed response variable. We excluded zero data from the density models. To calculate a density for each H&E-stained tissue and mechanoreceptor type, we summed counts for each identified mechanoreceptor and divided by the relevant tissue area. To calculate proportion for each quadrant and mechanoreceptor type along the proximodistal axis in each tissue, we divided the mechanoreceptor count in the quadrant by the total mechanoreceptor count of that type in the tissue.

We used R and multcomp (Hothorn, Bretz, & Westfall, 2008) to test a series of post hoc hypotheses using custom contrasts with equal weighting to compare presence, density, and proportion for each mechanoreceptor type and to compare total thickness of the epidermis and each epidermal layer separately across glabrous skin region and ROI. Using custom contrasts allowed us to assess whether the variable of interest was greater in the paw or ROIs of the paw after generally assessing the difference in means across the nonbinary fixed effects of glabrous skin regions and of ROIs. We did not use custom contrasts for the left-right laterality model, since we could assess the binary fixed effect within the GLMM. If we received convergence warnings on a model, we used allFit in the lme4 package to assess if model fit differed significantly with different optimizers. If log-likelihoods for each optimizer were within thousandths of a decimal point, we determined that the optimizer did not influence parameter estimates. To control the family-wise Type 1 error rate given multiple contrasts we used a reversed sequential Bonferroni procedure, which firsts tests the largest p value within a family of tests at the significance level (Hochberg, 1988). If not significant, we tested the next largest p -value within the family at the significance level for that test divided by 2. If not significant, we tested the next largest p -value within the family at the significance level for that test divided by 3, and so on. When the first significant test was reached, we considered all tests with p values less than that critical value as significant.

3 | RESULTS

3.1 | Gross description of glabrous skin regions and ROIs

Although the palmar paw pad is considered a glabrous skin region, hair was distributed on the pad in predictable patterns. Short guard hairs were sparsely distributed at the base of the digit pads and extended into the crease to the distal palmar pad (Figure 1a,b). Longer guard hairs were distributed across the proximal half of the proximal metacarpal pad and extended into the crease to the ulnar carpal pad (Figure 1a). In the paw, the glabrous surface extended distally past the claws and wrapped the distal tips to cover the dorsal side of the distal digits (Figure 1c). In the flipper, this pattern was reversed: the claw extended distally past the glabrous surface, which was entirely volar and separated from the claw by a slender band of hair (Figure 1d).

Epidermal surface texture varied greatly within and between glabrous skin regions (Figure 2). Surface texture varied along the proximodistal axis across the paw pad and the paw pad digits (Figures 1a and 2a). The ulnar carpal pad comprised regular, rounded protrusions arranged in transverse ridges along the diagonal axis; ridges were separated by shallow grooves (Figure 1a). The palmar pads showed short, narrow, rounded protrusions separated by wide, shallow valleys with no discernable ridged pattern (Figure 1a). The digits showed dense packing of tall, wide, molariform protrusions separated by deep, narrow valleys with no discernable ridged pattern; protrusion size varied, and sometimes one protrusion contained additional rounded projections (Figures 1a,b and 3a). The surface texture of the paw was consistent with the structure of the epidermal–dermal interface, visible histologically as deep, narrow, tightly packed rete ridges interdigitated with deep, narrow dermal papillae (Figure 2a).

Surface texture of the flipper plantar pad was similar to the ulnar carpal pad, but at high magnification, the protrusions appeared to have a more subtle molariform shape than those on the paw digits (Figures 1d and 3a,b). Surface texture of the flipper pad was consistent with the structure of the epidermal–dermal interface, visible histologically as shallow, wide ridges interdigitated with shallow, wide dermal papillae (Figure 2b). Surface texture of the rhinarium pad comprised relatively smooth skin with slight creasing around its perimeter and the nostrils; short, wide, flattened protrusions were tightly packed in the ventral (lower) half, and taller, more rounded protrusions were less dense in the dorsal (upper) half (Figures 2c and 3c). In contrast to the flipper and paw digit pads, the surface texture in the rhinarium was not

consistent with the structure of the epidermal–dermal interface visible histologically: shallow, wide rete ridges interdigitated with shallow, narrow dermal papillae (Figure 2c). Surface texture of the lip comprised smooth skin organized in ridges similar in height to the skin around the rhinarium's perimeter and nostrils, and microridges were apparent at high magnifications (Figures 2d and 3d). In contrast to the flipper and paw digit pads but consistent with the rhinarium pad, the smooth surface texture in the lips was not consistent with the structure of the epidermal–dermal interface visible histologically: shallow, narrow rete ridges interdigitated with shallow, narrow dermal papillae (Figure 2d).

The flipper, rhinarium, and paw pads displayed the five typical mammalian glabrous epidermal layers (stratum corneum, stratum lucidum, stratum granulosum, stratum spinosum, and stratum basale), but the lips lacked the stratum lucidum (Figure 4). We found minimal to no significant effects of laterality (e.g., left or right sides of the body) for absolute measures of total epidermal thickness and epidermal layer thickness in the paw or flipper digit pad (Tables S7 and S8). Given the lack of lateral effect for these glabrous skin regions we did not control for laterality in subsequent analyses of patterns in absolute and proportional thickness.

Since tissues often tore along the dermal–hypodermal boundary during histological processing, we could not reliably quantify how dermal thickness differed between glabrous skin regions.

Differences in skin thickness were apparent between glabrous skin regions during tissue preparation. Relative to other glabrous skin regions, the paw's thick integument quickly dulled the scalpel blades and was underlaid by substantial connective tissue, musculature, and bones. Microscopic measurements of total epidermal thickness and epidermal layer thickness in tissues confirmed gross differences observed during tissue preparation: total epidermal thickness was highest in the paw, with the digits and distal palm showing significantly thicker epidermis than other paw pad ROIs (Figure 4a and Tables 1 and S1–S3). This pattern primarily reflected a disproportionately thicker stratum

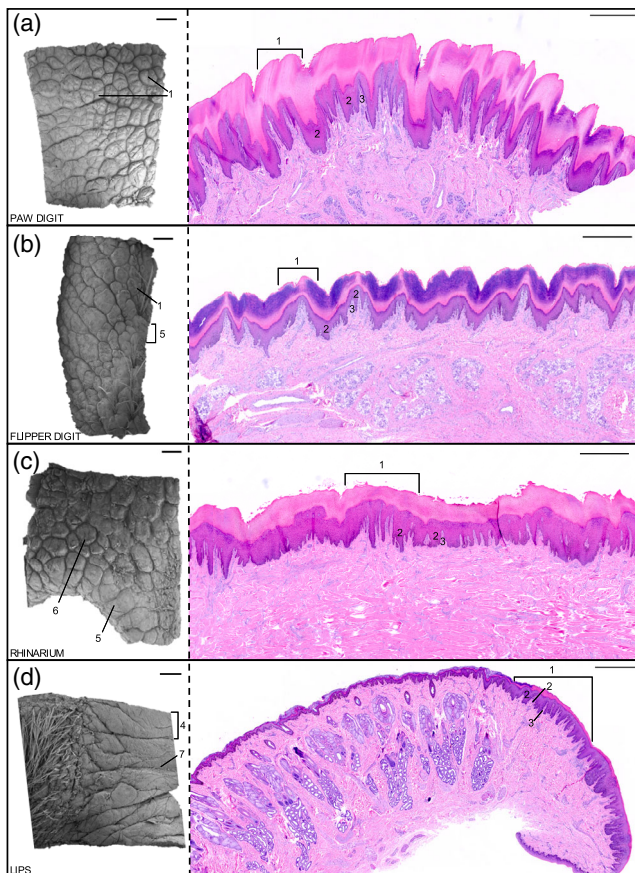


FIGURE 2 Samples of sea otter skin from glabrous skin regions—(a) digit 3 of right palmar paw, (b) digit 3 of right plantar flipper, (c) right rhinarium pad, (d) right dorsal (upper) lip—imaged via scanning electron microscopy (left panel) and light microscopy of transverse sections (right panel, hematoxylin and eosin [H&E] stain); scale bars = 1 mm for both image types. Surface texture differed for all glabrous skin regions. (a) For the paw digit pad, tall, narrow, round protrusions were densely packed with no discernable ridged pattern. Protrusions were often molariform with additional rounded projections (1); an enlarged view of the molariform shape is provided in Figure 3. This surface texture was consistent with the structure of the epidermal–dermal interface visible histologically (right panel): tightly packed deep, narrow ridges (2) interdigitated with deep, narrow dermal papillae (3). (b) For the flipper digit pad, wide protrusions—some of which displayed a subtle molariform shape (1)—were densely packed and organized in diagonal transverse ridges (4); an enlarged view of the subtle molariform structure is provided in Figure 3. This surface texture was consistent with the structure of the epidermal–dermal interface visible histologically (right panel): shallow, wide ridges (2) interdigitated with shallow, wide dermal papillae (3). (c) For the rhinarium pad, wide protrusions transitioned from short and flat (5) around the nostril to taller and more rounded (6) dorsally (in the upper half); an enlarged view of the rounded protrusion is provided in Figure 3. This surface texture was not consistent with the structure of the epidermal–dermal interface visible histologically (right panel): shallow, wide ridges (2) were not well differentiated and interdigitated with shallow, narrow dermal papillae (3). (d) For the lips, smooth skin was organized in wide ridges (4) oriented perpendicular to the hair boundary, with some shallow transverse creases (7). The labial ridges were similar in height to the protrusions on the rhinarium pad near the nostrils (5, (e) left panel), and additional microridges were scattered in each ridge; an enlarged view of the microridges is provided in Figure 3. This surface texture was not consistent with the structure of the epidermal–dermal interface visible histologically (right panel): shallow, narrow ridges (2) were not well differentiated and interdigitated with shallow, narrow dermal papillae (3)

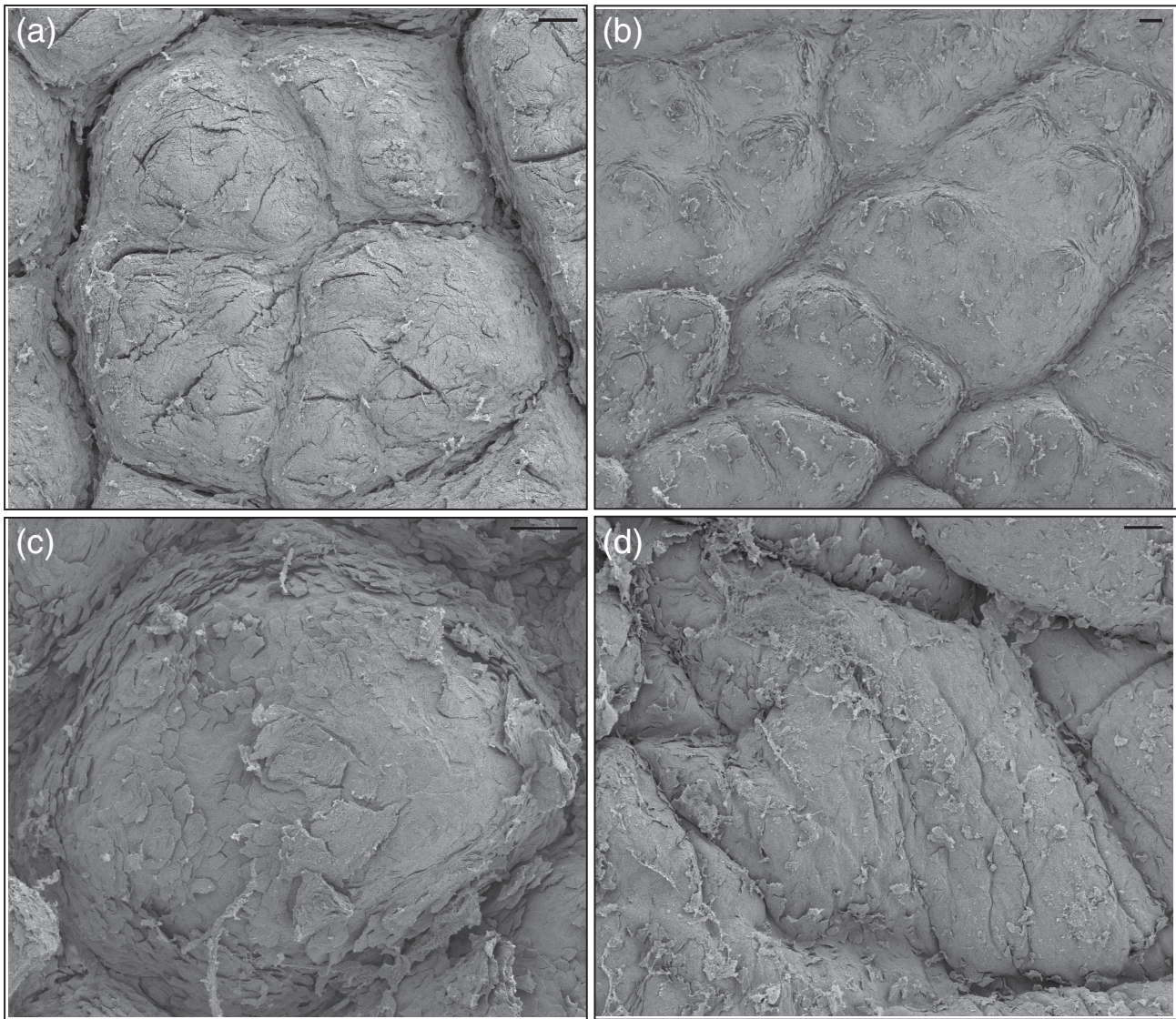


FIGURE 3 High-magnification scanning electron micrographs of skin-surface texture in glabrous skin regions of the sea otter: (a) molariform protrusion characteristic of the palmar paw digits, (b) protrusions with more subtle molariform shapes on the plantar flipper digit pad relative to the paw digit pad, (c) rounded protrusion in the dorsal rhinarium, and (d) microridges intersecting wide, flat ridges in the lips (scale bars = 100 μm for all images). Surface contamination appears as web-like fibrils

corneum in the digits and distal palm of the paw relative to other paw pad ROIs or glabrous skin regions; thickness of other epidermal layers remained proportional in the glabrous skin regions showing five epidermal layers (i.e., the paw, flipper, and rhinarium; Figure 4b and Tables S4–S6). In models comparing skin thickness between glabrous skin regions, the random effect of variation between individual sea otters explained 18.6% of the total unexplained variance for absolute epidermal thickness and 27.6, 19.4, 38.0, 16.0, and 23.2% for absolute thickness of the stratum corneum, stratum lucidum, stratum granulosum, stratum spinosum, and stratum basale, respectively (Table S2); this suggests that identifying additional predictor variables may improve overall fit of the

models to the observed data. In models comparing skin thickness within the paw pad ROIs, the random effect of variation between individual sea otters explained 44.0% of the total unexplained variance for absolute epidermal thickness and 44.5, 60.0, 61.3, 36.0, and 14.6 for absolute thickness of the stratum corneum, stratum lucidum, stratum granulosum, stratum spinosum, and stratum basale, respectively (Table S3); this suggests that, for some models, the predictor variables contributed a relatively good fit to the observed data and for other models, identifying additional predictor variables may improve overall fit to the observed data.

The hair that occurred along the boundaries of glabrous skin regions and some paw ROIs showed typical

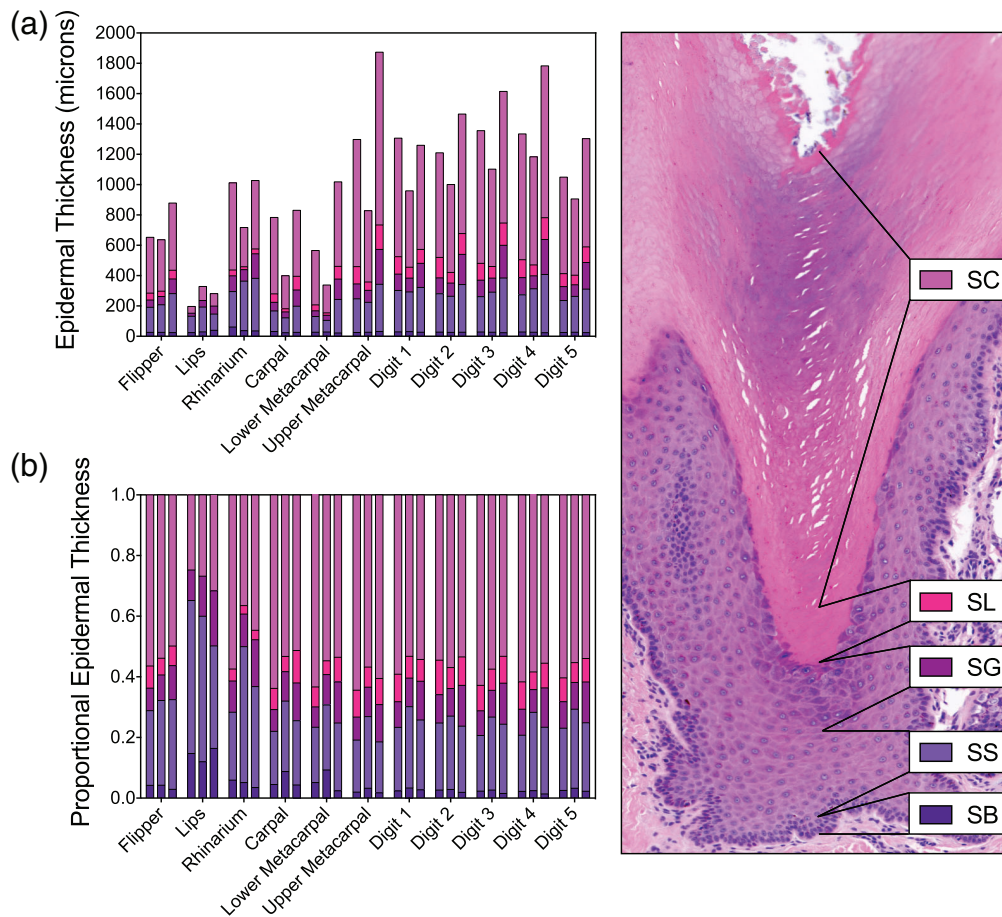


FIGURE 4 (a,b) Total epidermal thickness (μm), plotted separately by epidermal layer, and proportional thickness of each epidermal layer as determined in hematoxylin and eosin (H&E)-stained paraffin sections of glabrous skin regions from sea otters: (right panel) stratum corneum (SC), stratum lucidum (SL), stratum granulosum (SG), stratum spinosum (SS), and stratum basale (SB). All epidermal layers were present in the flipper, rhinarium, and paw pads, but the stratum lucidum was not apparent in the lips (a,b). The epidermis and proportional stratum corneum thickness were thickest in the distal metacarpal and five digits of the paw pad (a), but thicknesses of other epidermal layers were mostly proportional across the glabrous skin regions containing all five epidermal layers (i.e., flipper, rhinarium, and paw pads (b))

morphology for guard hair: each hair shaft was surrounded by an internal root sheath, an external root sheath, a glassy membrane, and a perifollicular connective tissue sheath (Figure 5). Regardless of glabrous skin region, each hair follicle was associated with two lobulated sebaceous glands, one on either side and an apocrine sweat gland (Figure 5a). Apocrine sweat glands were found in all glabrous skin regions, but only in association with pilosebaceous units. Eccrine sweat glands occurred throughout the dermis of the paw and flipper, but not in the rhinarium or lips. In both the paw and flipper, eccrine sweat glands were inversely associated with pilosebaceous-apocrine units.

Variation in dermal innervation and circulatory structures was apparent between glabrous skin regions during qualitative observations of tissues. Gross dermal innervation appeared substantially higher in the digit

pads, distal palmar pads, and ulnar carpal pad of the paw than in the flipper pad, lips, or rhinarium pad. We also noted a higher proportion of vascular profiles in the same areas of the paw pads, including dense aggregations of arteriovenous anastomoses, capillaries, and glomus bodies, especially in the superficial dermis (Figure 6b).

3.2 | Gross description of mechanoreceptor types and distribution

We confirmed the presence of Merkel cells and Pacinian corpuscles based on morphology in sea otter glabrous skin, but we did not observe structures resembling typical Meissner corpuscles. Merkel cells in sea otters showed a characteristic oval shape with a large nucleus and pale-

TABLE 1 Mean density and *SD* of total epidermal thickness, absolute epidermal layer thickness, and proportional epidermal layer thickness across regions of interest (ROIs) and glabrous skin regions, estimated from 12 measurement points in each replicate (hematoxylin and eosin [H&E]-stained, slide-mounted tissues) obtained from three sea otters

Glabrous skin region	ROI	Replicates (H&E-stained tissues)	Total epidermal thickness (microns)		Absolute epidermal layer thickness (microns)			Proportional epidermal layer thickness		
			\bar{x}	σ	\bar{x}	σ		\bar{x}	σ	
Flipper	—	12	722.71	210.19	SC	383.41	128.64	SC	0.56	0.07
					SL	46.21	25.21	SL	0.08	0.04
					SG	66.10	30.53	SG	0.10	0.03
					SS	201.37	89.82	SS	0.24	0.06
					SB	25.62	9.31	SB	0.03	0.02
Lips	—	6	268.91	156.97	SC	73.11	61.39	SC	0.55	0.09
					SL	—	0.00	SL	0.09	0.05
					SG	38.72	30.51	SG	0.10	0.04
					SS	126.26	90.53	SS	0.23	0.08
					SB	30.83	15.26	SB	0.03	0.01
Paw	D1	11	1,167.31	361.52	SC	654.55	237.54	SC	0.53	0.10
					SL	93.17	49.28	SL	0.06	0.03
					SG	115.34	49.47	SG	0.09	0.03
					SS	275.03	104.47	SS	0.27	0.08
					SB	29.23	12.38	SB	0.04	0.02
Paw	D2	11	1,203.21	406.86	SC	675.74	281.95	SC	0.56	0.09
					SL	110.15	60.48	SL	0.08	0.04
					SG	125.61	65.83	SG	0.10	0.03
					SS	264.88	106.24	SS	0.21	0.07
					SB	26.84	9.04	SB	0.06	0.05
Paw	D3	9	1,357.96	430.51	SC	795.37	305.20	SC	0.57	0.08
					SL	111.58	58.27	SL	0.06	0.03
					SG	138.45	73.43	SG	0.10	0.04
					SS	286.47	116.42	SS	0.21	0.07
					SB	26.09	8.89	SB	0.06	0.04
Paw	D4	12	1,433.56	450.65	SC	847.54	316.10	SC	0.56	0.07
					SL	111.38	52.97	SL	0.07	0.03
					SG	143.06	82.85	SG	0.10	0.03
					SS	305.30	113.40	SS	0.23	0.07
					SB	26.27	7.75	SB	0.03	0.01
Paw	D5	12	1,086.84	383.20	SC	617.55	241.52	SC	0.61	0.06
					SL	83.93	47.60	SL	0.08	0.03
					SG	114.89	63.15	SG	0.10	0.03
					SS	245.14	101.69	SS	0.19	0.05
					SB	25.34	8.20	SB	0.02	0.01
Paw	DM	12	1,333.21	489.25	SC	815.89	325.49	SC	0.58	0.09
					SL	110.41	60.47	SL	0.08	0.03
					SG	135.70	81.45	SG	0.10	0.04
					SS	243.58	76.56	SS	0.22	0.07
					SB	27.63	10.01	SB	0.02	0.01
Paw	PM	9	640.55	371.43	SC	366.32	223.78	SC	0.28	0.16
					SL	46.08	38.17	SL	0.00	0.00
					SG	68.57	53.83	SG	0.14	0.06
					SS	133.77	85.92	SS	0.44	0.19
					SB	25.81	11.66	SB	0.14	0.08
Paw	CP	12	668.88	347.50	SC	382.99	214.76	SC	0.59	0.08
					SL	55.82	48.68	SL	0.08	0.03
					SG	67.74	48.63	SG	0.10	0.04
					SS	135.21	76.47	SS	0.22	0.07
					SB	27.13	12.54	SB	0.02	0.01

TABLE 1 (Continued)

Glabrous skin region	ROI	Replicates (H&E-stained tissues)	Total epidermal thickness (microns)		Absolute epidermal layer thickness (microns)		Proportional epidermal layer thickness			
			\bar{x}	σ	\bar{x}	σ	\bar{x}	σ		
Rhinarium	—	3	918.56	244.11	SC	427.93	168.26	SC	0.46	0.13
					SL	29.66	15.22	SL	0.03	0.02
					SG	113.98	66.40	SG	0.12	0.05
					SS	302.54	126.69	SS	0.34	0.13
					SB	44.45	31.58	SB	0.05	0.02

Note: Paw ROIs include ulnar carpal pad (CP), proximal metacarpal pad (PM), distal metacarpal pad (DM), and five digit pads (D1–D5). Epidermal layers include stratum corneum (SC), stratum lucidum (SL), stratum granulosum (SG), stratum spinosum (SS), and stratum basale (SB).

staining cytoplasm (Figure 6a). The spatial association of Merkel cells relative to rete ridges or dermal papillae could be reliably identified (92.4%, 2,353/2,547). Merkel cells were located in the stratum basale, almost always occurring at the base of rete ridges (93.7%, 2,204/2,353 Merkel cells) and rarely spatially associated with dermal papillae (0.2%, 5/2,353). Occasionally Merkel cells were not clearly associated with either rete ridges or dermal papillae (6.1%, 144/2,353). We typically found close spatial associations between Merkel cells in the stratum basale and discoid nerve terminals innervated with myelinated afferent nerve fibers in the superficial dermis (Figure 6b). Merkel cells were occasionally found alone (7.7%, 196/2,547, Figure 6a, left panels), but were usually found in clusters (2,351/2,547, 92.3%, Figure 6a, right panels). The number of Merkel cells per cluster varied from 2 to 32, with a mean of 10.8 ± 6.5 cells/cluster. Clusters comprised cells that were either clumped across multiple cell layers of the stratum basale or spread out linearly along the stratum basale (Figure 6a). Whether clustered or not, the cross-sectional area occupied by individual Merkel cells remained consistent ($113.26 \pm 34.6 \mu\text{m}^2$). Merkel cells tended to be oriented with the long axis aligned parallel to the basement membrane. We did not find Merkel cells associated with hair follicles sparsely distributed in some glabrous skin regions.

Pacinian corpuscles in sea otters comprised an inner unmyelinated neurite surrounded by concentric non-neuronal lamellae (Figure 6). Pacinian corpuscles were present in the superficial dermis and at the boundary between the dermis and hypodermis. The spatial association of Pacinian corpuscles relative to rete ridges or dermal papillae could be reliably identified (91.0%, 365/401). Pacinian corpuscles were often spatially associated with dermal papillae (48.8%, 178/365 Pacinian corpuscles). They were less commonly associated with rete ridges (21.9%, 80/365), or not clearly associated with either rete ridges or dermal papillae (29.6%, 108/365). Pacinian

corpuscles were found alone (203/401, 50.6%, Figure 6b, left panels) and in clusters (49.4%, 198/401, Figure 6b, right panels), in which the number of corpuscles per cluster varied from 2 to 8 with a mean of 3.0 ± 1.4 . The cross-sectional size of Pacinian corpuscles varied more than Merkel cells (area: $0.0375 \pm 0.0564 \text{ mm}^2$, maximum length: $0.368 \pm 0.169 \text{ mm}$). Pacinian corpuscles were less clearly oriented relative to the basement membrane than Merkel cells; the long axis of each Pacinian corpuscle was sometimes perpendicular and sometimes parallel to the stratum basale.

Our identification and subsequent counts of mechanoreceptor types were consistent and conservative; we only counted cells or corpuscles that we could confidently identify based on morphology. In addition to classic morphology of Merkel cells and Pacinian corpuscles, we found many unmyelinated afferent nerve fibers surrounded by lamellae that resembled the inner core of Pacinian corpuscles. These structures either occurred as a single unit or as a cluster of distinct neurites, each surrounded by lamellae but connected within a single encapsulation that resembled the outer core of a Pacinian corpuscle. We also found structures identical to this description, except they lacked a central unmyelinated afferent nerve fiber. These unidentified neural structures were often concentrated in the superficial dermis and showed a qualitatively higher density in the digit pads, distal palmar pad, and ulnar carpal pad of the paw than in the flipper pad, lips, or rhinarium pad. We suspect that they comprise free nerve endings, ends of Pacinian corpuscles, and encapsulated nerve endings of other mechanical or thermal receptors. These uncategorized nerve fibers extended from the deep dermis to the stratum basale, where they followed along one or both side(s) of a rete ridge into the dermal papillae. Merkel cells, Pacinian corpuscles, and the uncategorized neural structures were all spatially associated with arteriovenous anastomoses and capillaries (Figure 6).

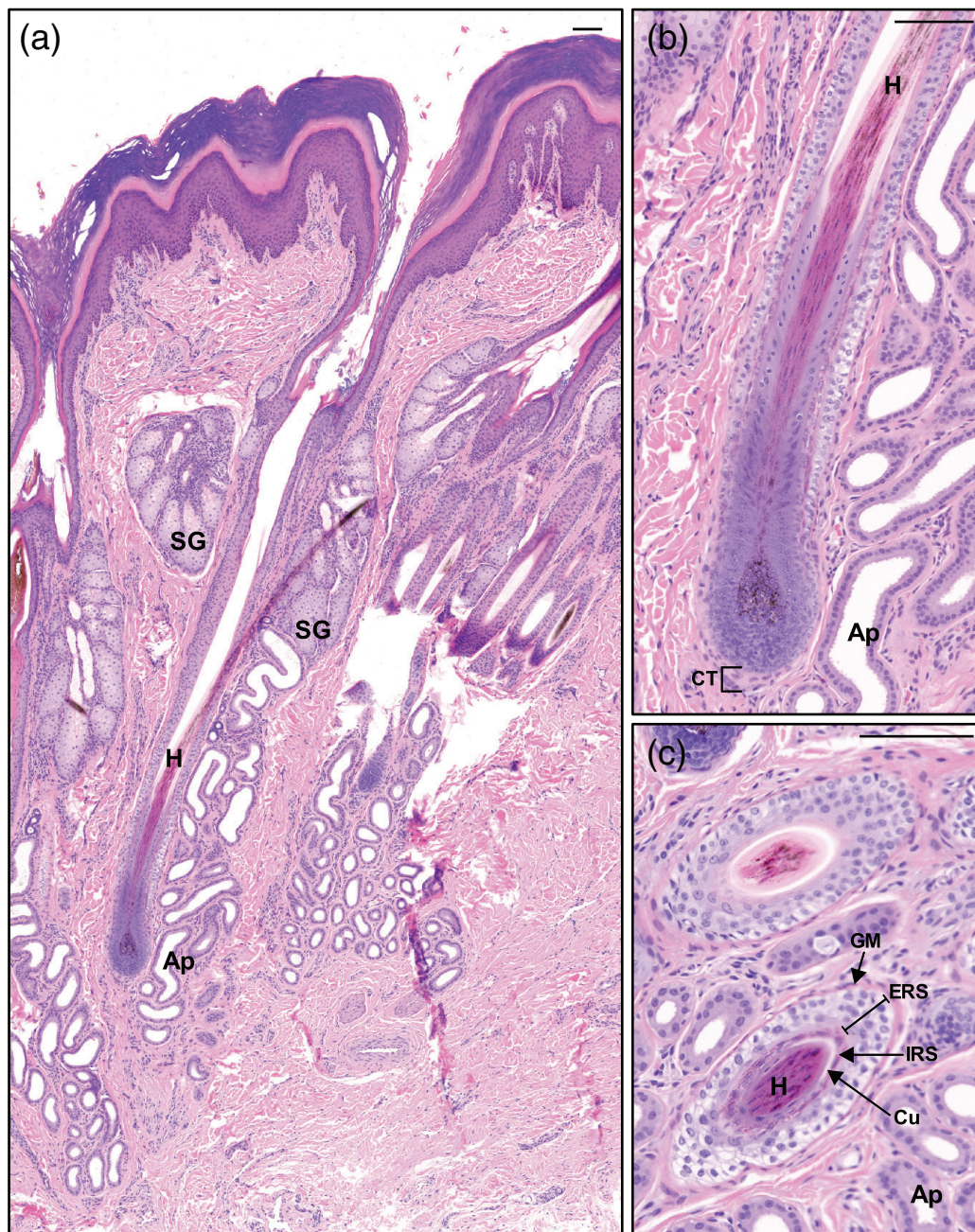


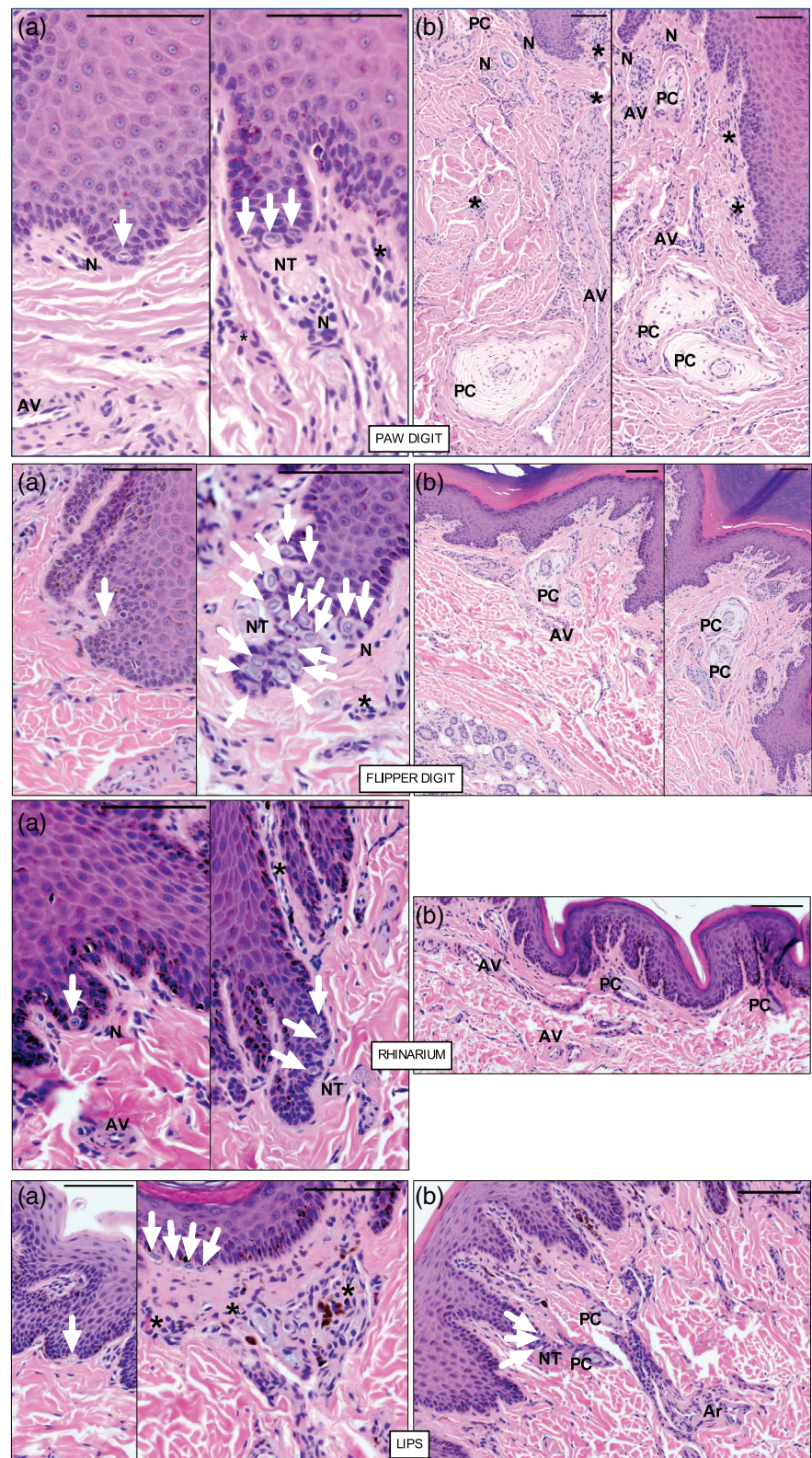
FIGURE 5 Guard hair shaft (H) within hair follicle from hematoxylin and eosin (H&E)-stained paraffin section of sea otter glabrous skin: (a,b) sectioned longitudinally from digit 1 of the right palmar paw pad, and (c) in cross-section from digit 3 of the left plantar flipper pad (scale bars = 100 μ m). Each hair follicle is associated with two lobulated sebaceous glands (SG) and an apocrine sweat gland (Ap), whose duct empties into the hair follicle. A connective tissue sheath (CT) surrounds the glassy membrane (GM) of the external root sheath (ERS). Moving inwards, the internal root sheath (IRS) surrounds the pale-staining cuticle layer (Cu) that encompasses the hair shaft (H)

3.3 | Variation in mechanoreceptor presence and density

Merkel cells were observed microscopically in the majority of tissues for all glabrous skin regions (Table 2). Pacinian corpuscles were observed in at least one tissue in all glabrous skin regions; the proportion of

tissues containing at least one Pacinian corpuscle varied between and within glabrous skin regions (16.7–100%, Table 2), but this variation was not statistically significant (Table S9). In contrast to presence–absence patterns, the relative density of Merkel cells and Pacinian corpuscles varied substantially and significantly between glabrous skin regions (Figure 7 and Tables 2,

FIGURE 6 Hematoxylin and eosin (H&E)-stained paraffin sections from the paw digit pad, flipper digit pad, rhinarium pad, and lips that demonstrate morphology and distribution of Merkel cells (a, arrows) and Pacinian corpuscles (b, PC) in sea otter glabrous skin regions; scale bars = 100 μ m. Arteriovenous anastomoses (AV), capillaries (*), and large myelinated sensory nerves (N), were closely associated with both mechanoreceptor types and extended superficially to the epidermis. (a) Merkel cells (arrows) were distributed along the stratum basale as either solitary cells (left panel) or a cluster (right panel). Often afferent nerve fibers leading to the discoid nerve terminal (NT) were apparent in the superficial dermis in close association with the Merkel cells. (b) Pacinian corpuscles (PC) were distributed in the deep and superficial dermis as either solitary cells (left panel) or a cluster (right panel)



S10, and S11). Merkel cell density in the paw was significantly higher than any of the other glabrous skin regions, and Pacinian corpuscle density in the paw was significantly higher than in the flipper pad and the rhinarium pad (Figure 7). Pacinian corpuscle density

was also higher in the paw pad relative to the lips, but since we observed Pacinian corpuscles in only one tissue of the lips, we had low statistical power for this contrast (Figure 7b). The random effect of variation between individual sea otters explained 23.7% of the total

Glabrous skin region	ROI	Replicates (H&E-stained tissues)	Merkel cells		Pacinian corpuscles	
			Mean cell density (count/mm)	SD	Mean cell density (count/mm ²)	SD
Flipper	—	12	0.44	0.44	0.04	0.05
Lips	—	6	0.18	0.09	0.01	0.03
Paw	D1	11	0.66	0.63	0.05	0.03
Paw	D2	11	0.81	0.54	0.10	0.08
Paw	D3	9	0.59	0.38	0.12	0.07
Paw	D4	12	0.63	0.53	0.11	0.07
Paw	D5	12	0.88	0.77	0.11	0.09
Paw	UM	12	0.80	0.93	0.05	0.05
Paw	LM	9	0.04	0.07	0.01	0.02
Paw	CP	12	0.56	0.45	0.01	0.02
Rhinarium	—	3	0.09	0.02	0.00	0.01

Note: Paw ROIs include ulnar carpal pad (CP), proximal metacarpal pad (PM), distal metacarpal pad (DM), and five digit pads (D1–D5).

TABLE 2 Mean density and *SD* of Merkel cells and Pacinian corpuscles across glabrous skin regions and regions of interest (ROIs), estimated from replicates (hematoxylin and eosin (H&E)-stained, slide-mounted tissues) obtained from three sea otters

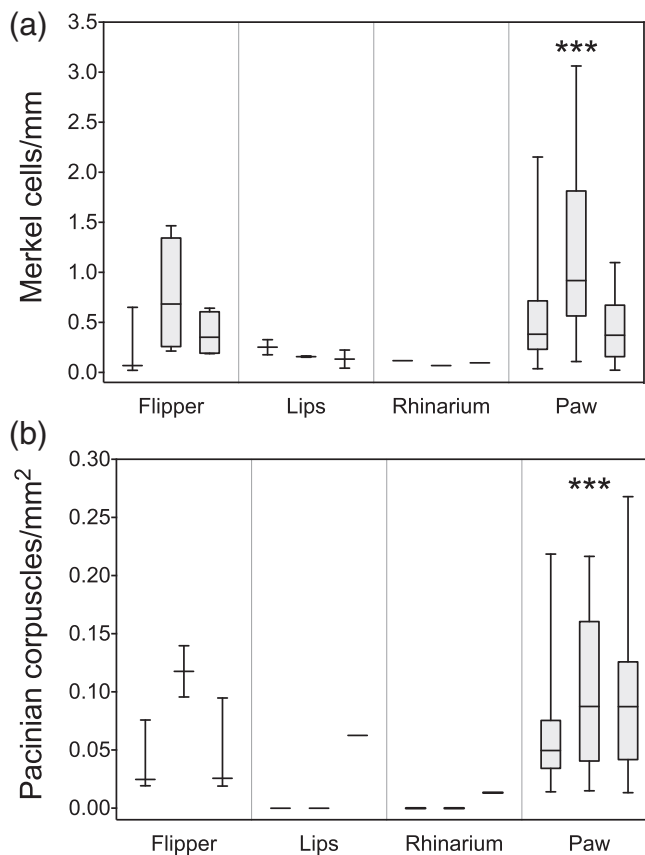


FIGURE 7 Absolute densities of mechanoreceptors across glabrous skin regions with density >0, plotted separately across individual sea otters. Despite variability in the paw and across sea otters, Merkel cell density (a) and Pacinian corpuscle density (b) were significantly higher in the paw than in all other glabrous skin regions (***p* < .001)

unexplained variance for Merkel cell density and 14.8% of the total unexplained variance for Pacinian corpuscle density (Table S11), which suggests that identifying additional predictor variables may improve overall fit of the models to the observed data.

As in the absolute measures of total epidermal thickness and epidermal layer thickness, we found no significant effects of laterality (e.g., left or right sides of the body) for presence or nonzero density of Merkel cells or Pacinian corpuscles in the paw pad or flipper digit pad (Tables S12 and S13). Given the lack of lateral effect for these glabrous skin regions we did not control for laterality in subsequent analyses of variation in density.

The relative densities of Merkel cells and Pacinian corpuscles varied across paw pad ROIs, with the digits and distal palm showing significantly higher densities for both mechanoreceptor types (Table 2 and Table S14). The four longest digits (D2, D3, D4, and D5) showed especially high densities, about two-thirds more than other ROIs in the paw pad. The random effect of variation between individual sea otters explained 70.9% of the total unexplained variance for Merkel cell density and 60.5% of the total unexplained variance for Pacinian corpuscle density (Table S14), which suggests that the predictor variables contributed a relatively good fit of the models to the observed data. The distal portions of the five digits showed a significantly higher proportional density for both Merkel cells and Pacinian corpuscles relative to the proximal portions of the digits (Figure 8 and Tables S15 and S16). In contrast, proportional density of both

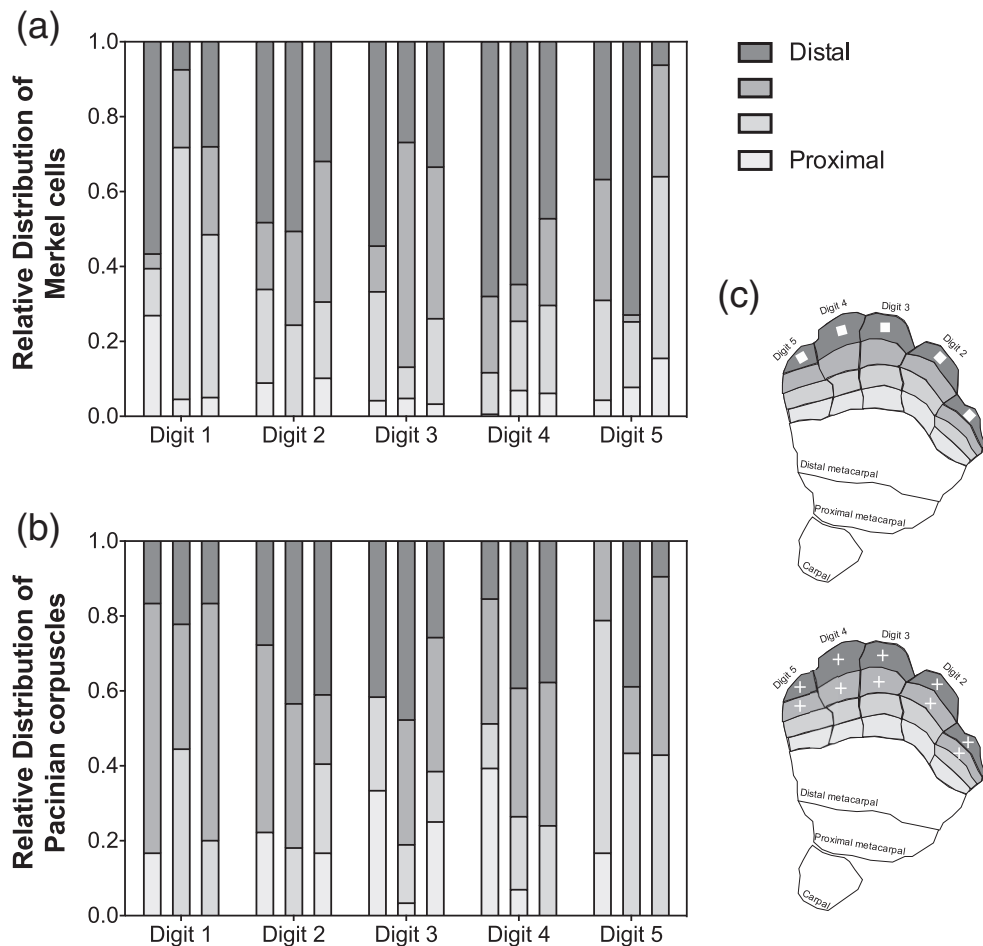


FIGURE 8 Proportional densities of mechanoreceptors across proximodistal quadrants of paw digit pads (light gray to dark gray-shaded areas), plotted separately for individual sea otters. Despite variability across sea otters, relative Merkel cell density (a) and relative Pacinian corpuscle density (b) increased significantly along the proximodistal axis when tested across two contrasts (c). Contrasts, represented by presence and absence of symbols (■ and +), are illustrated for the right paw (c), but analyses correspond to combined relative densities from left and right paws. The relative density of each mechanoreceptor type was significantly higher in the most distal digit quadrant when contrasted to the other digit quadrants (■, $p < .01$ for Merkel cell relative density and $p < .05$ for Pacinian corpuscle relative density), and significantly higher in the distal half of the digits when contrasted to the proximal half of the digits (+, $p < .01$ for Merkel cell relative density and $p < 0.001$ for Pacinian corpuscle relative density)

mechanoreceptor types did not significantly vary along the proximodistal axis in the metacarpal pads, ulnar carpal pad, or flipper digit pad (Table S15).

4 | DISCUSSION

The results from this anatomical study complement behavioral assessments of active touch (Strobel et al., 2018) to enable a more complete understanding of the sense of touch in a semi-aquatic carnivore. Densities of Merkel cells and Pacinian corpuscles were greater in the paw than in other glabrous skin areas, which indicate that paws are the primary sites of active touch across all glabrous skin regions in sea otters. The distal paw—especially the distal digits—likely functions as a tactile

fovea in sea otters, both for spatial resolution and detection of high-frequency vibrations transmitted to the skin from objects held in the paw (Johnson, 2001; Johnson & Hsiao, 1992). This perspective is supported by our detection of variation in densities of Merkel cells and Pacinian corpuscles along the proximodistal axis in the paw pad, with highest densities in the distal metacarpal pad and the longest four digits; this pattern is absent in the proximal metacarpal pad and ulnar carpal pad. Our observations of the relative distribution of mechanoreceptors coincide with the behavioral strategy used by a sea otter in controlled measures of tactile discrimination, in which the sea otter preferentially used the digits and distal metacarpal pad to explore textured stimuli (Strobel et al., 2018). Our data are also supported by observational studies of wild sea otter behavior during tactile

exploration, object manipulation, prey handling, and tool use (Fujii, Ralls, & Tinker, 2015; Hall & Schaller, 1964).

The morphology of Pacinian corpuscles and Merkel cells in sea otters is consistent with those described for other mammals (Bell et al., 1994; Halata, 1990; Iggo & Andres, 1982; Merkel, 1875; Young et al., 2014) and the Merkel-cell-like structures previously noted in the flipper digit pads of sea otters (Williams et al., 1992). Although spatial association between Merkel cells and the stratum basale is consistent with the “typical” mammalian pattern, small Pacinian corpuscles were commonly observed in the superficial dermis of sea otters in close proximity to the stratum basale. A similar pattern for Pacinian corpuscles has been reported for the trunk tip of Asian elephants (Rasmussen & Munger, 1996), but the authors noted that the pattern was unusual relative to descriptions for marsupials and placental mammals, including humans and primates (Halata, 1990).

We did not find definitive Meissner corpuscles in sea otter glabrous skin. This result is not particularly surprising, since Meissner corpuscles have primarily been reported and described in a small number of mammalian species: in the palms, foot soles, lips, and oral mucosae of primates, some rodents, marsupials, and elephants (Hoffmann, Montag, & Dominy, 2004; Ide, 1977; Munger & Ide, 1988; Tachibana & Fujiwara, 1991; Verendeev et al., 2015; Weissengruber et al., 2006; Winkelmann, 1964). However, we did find substantial encapsulated and unencapsulated neural structures distributed in the superficial dermis of the paw relative to other glabrous skin areas. These structures resembled Pacinian corpuscles and “Meissner-like” structures described in the trunks of African and Asian elephants (Hoffmann et al., 2004; Rasmussen & Munger, 1996) and the footpads of cats and mice (Bolanowski & Pawson, 2003; Gonzalez-Martinez et al., 2004), as well as a heterogeneous grouping of “simple corpuscles” described in the footpads of raccoons (Munger & Pubols, 1972; Rice & Rasmusson, 2000) and squirrels (Brenowitz, 1980). Consistent with conclusions in these studies, we suspect that the uncategorized neural structures in sea otters contribute to tactile sensitivity due to their proximity to the epidermis and close association with rete ridges and dermal papillae. Alternatively, the uncategorized neural structures may function with circulatory features to regulate heat flux (see *Epidermal thickness, texture, and the aquatic environment*). Overall, the combination of dense Merkel cells, superficially distributed Pacinian corpuscles, and uncategorized neural tissue may explain the sensitive touch measured in sea otters (Strobel et al., 2018) despite the absence of defined Meissner corpuscles.

4.1 | Mechanoreceptor density and distribution

Direct comparison of absolute mechanoreceptor densities of the sea otters in this study to species in other studies is difficult and questionably informative given methodological differences, so we offer a comparison of relative densities and patterns. The proximodistal increase of mechanoreceptor density in the sea otter paw is qualitatively similar to patterns observed in the hands of humans and nonhuman primates (Johansson & Vallbo, 1979; Kumamoto, Senuma, Ebara, & Matsuura, 1993; Paré et al., 2002; Stark, Carlstedt, Hallin, & Risling, 1998), the forefeet of cats (Kumamoto, Takei, Kinoshita, Ebara, & Matsuura, 1993) and the elephant trunk (Rasmussen & Munger, 1996). However, Pacinian corpuscles are more evenly distributed across the hand in humans (Johansson & Vallbo, 1979) than in the paws of sea otters, which may relate to the different ways in which sea otters and humans grasp objects. Proximodistal patterns in mechanoreceptor density were also less apparent in the feet of Asian elephants and the paws of tree squirrels (Bouley, Alarcón, Hildebrandt, & O’Connell-Rodwell, 2007; Brenowitz, 1980) than in the paws of sea otters, which may relate to the different ways in which sea otters and these species position their extremities to detect tactile cues and/or manipulate objects. Although this study used a sampling design that allowed us to make intraspecific comparisons, a more intensive serial sectioning approach would allow quantification of absolute mechanoreceptor density and innervation density across glabrous skin regions. These data for adult sea otters would substantially help to place their degree of tactile specialization in a comparative context.

Sea otters show minimal densities of Merkel cells, Pacinian corpuscles, or Meissner-like corpuscles in the rhinarium and lips relative to other species (Halata & Munger, 1983; Lacour, Dubois, Pisani, & Ortonne, 1991), which coincide with observations of wild and captive sea otters’ tendency to explore objects with paws first, rarely approaching objects for face-first exploration. In the southern sea otter population, female nose trauma often results from intersexual aggression from males during breeding attempts (Staedler & Riedman, 1993). Although severe nose wounds can contribute substantially to the cause of death in this population (Chinn et al., 2016; Estes, Hatfield, Ralls, & Ames, 2003; Kreuder et al., 2003), little evidence so far suggests that death results from reduced foraging success due to reduced rhinarium skin sensitivity, as would be expected if tactile perception via the rhinarium were critical for prey detection or capture. In addition, in controlled, behavioral measurements tactile sensitivity, a trained sea otter was capable of

accurate and quick perception using her vibrissae even when her nose and lips did not contact the stimuli (Strobel et al., 2018). The combination of structural and behavioral observations do not discount that the rhinarium and lips process tactile cues, but it does suggest that these glabrous skin regions contribute minimally to sensitive touch abilities in sea otters.

Preliminary examinations of the glabrous skin from deceased sea otter fetuses and living young sea otter pups reveal marked difference from our observed distribution of Pacinian corpuscles and skin-surface texture (S.M. Strobel, personal observation). Mechanoreceptor distribution and density have been documented to change as mammals age (see, e.g., Bruce, 1980; Klatzky & Lederman, 2003; Nava & Mathewson, 1996; Venkatesan, Barlow, & Kieweg, 2015; Wickremaratchi & Llewelyn, 2006). Since assessing touch ability for fetuses and young pups in controlled settings is impossible or impractical, investigating the ontogenetic component from an anatomical perspective may help predict how changes in neural organization across development affect sea otter pup foraging ability.

4.2 | Epidermal thickness, texture, and the aquatic environment

In all mammals, the epidermis serves as a barrier against physical, chemical, and mechanical irritants and regulates heat and water flux. The presence of the typical five mammalian epidermal layers in the paw, flipper pad, and rhinarium in this study is consistent with previous descriptions of sea otter haired skin (Kenyon, 1969) and differs from the lack of stratum lucidum reported for glabrous skin on the sole of the Siberian weasel, *Mustela sibirica* (Sokolov, 1982). We measured a substantially thick epidermis in sea otter glabrous skin that ranged from four to 260 times thicker than reported for the epidermis in haired skin obtained from the facial region of one sea otter (Kenyon, 1969) and haired skin obtained from the withers and breast of two Eurasian otters, *Lutra lutra* (Sokolov, 1982). Our measurements of epidermal thickness in the sea otter flipper pad are similar to those reported for the glabrous hind soles of terrestrial mustelids (Sokolov, 1982); although Sokolov reported that epidermal thickness was higher in the front soles relative to hind soles of terrestrial mustelids, the sea otter paw epidermis is thicker than those reported for the front soles of terrestrial mustelids. Taken together, these comparisons suggest that increased epidermal thickness in sea otter paw pads is not due to an overall increase in epidermal thickness across haired or glabrous skin regions.

Given the abrasive benthic foraging habitat of sea otters and the extensive antipredator defenses of their hard-shelled invertebrate prey, the localized superkeratinization in the tactile-sensitive paw may defend against physical damage while capturing and handling prey (Rothman & Lorincz, 1963). Superkeratinization is common in the footpads of terrestrial mammals and the ventral skin surfaces used for locomotion in amphibious mammals (da Silva et al., 2020; Ling, 2018), but it has also been reported for the anterior facial skin of the walrus, an amphibious benthic feeder like the sea otter (Fay, 1982). The thicker epidermis in the distal metacarpal and digit pads in sea otters relative to other glabrous skin areas, primarily a result of a thicker stratum corneum rather than other epidermal layers, may indicate that these paw areas are more likely to be involved in active touch exploration and manipulation of objects, whether due to their most distal location and/or higher tactile sensitivity. In other mammals, epidermal thickness can be negatively correlated with touch specialization (Catania 2000), but this is clearly not the case for sea otters (Strobel et al., 2018). Determining whether increased neural investment in the paw is necessary to maintain sensitivity despite increased epidermal thickness, or if increased epidermal thickness is necessary to maintain the sensitivity of the paws given abrasive foraging habitat may be possible, albeit highly difficult, to tease apart in controlled longitudinal captive studies.

Our findings of well-developed rete ridges and dermal papillae in all glabrous skin areas of sea otters differ from those described for haired skin on these mammals (Kenyon, 1969). Deep rete ridges may have multiple functions in sea otters. Deep rete ridges can strengthen the epidermal–dermal interface, which may protect the skin from tearing under high shearing forces. While we did not consider collagen fiber alignment, such information would contribute to our understanding of the relationship between skin morphology and physical forces (i.e., shearing vs. loading) that different regions of glabrous skin regularly endure. In addition, deep rete ridges and their associated dermal papillae enable neural structures and blood flow to be closer to the skin surface, which likely improves tactile perception. When skin-surface texture closely resembles that of the underlying epidermis–dermis interface, as in the sea otter paw, localization and transmission of mechanical stimuli to mechanoreceptors may be improved (Cauna, 1985; Hamrick, 2001). Clear differences in glabrous skin-surface texture observed in this study merit further investigation to determine how they relate to thermoregulatory, structural, and/or sensory functions in sea otters, and whether consistent patterns occur across terrestrial, semi-aquatic, and aquatic mammals.

Although this study did not focus on assessing thermoregulatory properties of glabrous skin, we did observe qualitative variation between glabrous skin regions that may relate to heat flux in sea otters. We noted a thick hypodermis in the paw that was not present in other glabrous skin during tissue preparation and a qualitatively higher circulatory investment across the paw pad, including arteriovenous anastomoses, capillaries, and glomus bodies. The fat layer and circulatory features likely improve heat retention and vasoconstriction efficiency, respectively, via countercurrent heat exchange (Kellogg, 2006; Rothman & Lorincz, 1963). In addition, the circulatory features could assist with effective heat dissipation given the thick epidermis, as has been suggested for the ventral flippers of pinnipeds (da Silva et al., 2020). However, it is unclear how these circulatory features function together with neural investment to maintain tactile or proprioceptive function in the paw across thermal gradients. The relatively smaller circulatory investment observed in the glabrous skin of the flipper digit pads, lips, and rhinarium of sea otters may relate to their decreased neural investment and/or suggest that these structures play a minimal role in radiative heat flux. The tradeoff between retention of neural function in the periphery and heat in the core is especially interesting to examine in sea otters, given their high metabolism, amphibious lifestyle, and distribution in areas of year-round cold water. Recognized to have a minimal mammalian dive response, including peripheral vasoconstriction (Yeates, Williams, & Fink, 2007), maintenance of superficial blood flow while diving could preserve neural function in peripheral sensory organs for sea otters. Further analyses could examine capillary density and glandular structure in sea otters. In North America sea otters are distinctly split between a subarctic subspecies (*Enhydra lutris kenyoni*) and a temperate subspecies (*Enhydra lutris nereis*), and a comparison between these populations may improve understanding of how different climates drive differential selection in mammalian tactile form and function. Quantifying substantial observed variation in guard hair density on the palmar pads of the paw (S.M. Strobel, personal observation) within and between populations could inform how this variation affects sensitivity to mechanical stimuli and temperature tolerance.

Both eccrine and apocrine sweat glands were present in sea otter glabrous skin. We noted eccrine sweat glands only in the paw and flipper pads, in which they were distinctly confined to areas where hair did not occur. In human skin eccrine sweat glands dissipate heat, but in the volar pads of terrestrial mammals they primarily improve frictional gripping and tactile sensitivity by moistening the skin (Adams & Hunter, 1969; Adelman,

Taylor, & Heglund, 1975; Meyer, Bartels, Tsukise, & Neurand, 1990; Meyer & Tsukise, 1995; Stumpf, Künzle, & Welsch, 2004). The aquatic habitat reduces the need for sea otters to increase skin hydration, so determining whether these eccrine sweat glands are vestigial or functional requires a comparative approach across terrestrial and semiaquatic mustelids. The association of apocrine glands with pilosebaceous units in glabrous skin is consistent with previous reports for sea otter haired skin (Kenyon, 1969; Kuhn et al., 2010). In many mammals odorous secretions from these glands are effective in chemical communication (Mykytowycz, 1972), but given that sea otters are not known for territorial scent marking, the oily secretions from these glands are more likely to serve as waterproofing for the guard hairs that border glabrous skin regions and portions of the paw pad.

5 | CONCLUSIONS

This study assessed tactile sensitivity in sea otters using a histological approach to describe the morphology, density, and distribution of neural structures in four glabrous skin regions. Based on morphometric characteristics, we confirmed the presence of two common mammalian mechanoreceptors, Merkel cells and Pacinian corpuscles, and failed to confirm the presence of Meissner corpuscles. Variation in relative densities of mechanoreceptors between the paw pad, flipper pad, lips, and rhinarium suggests that the paw is the primary tactile sense organ for sea otters. An increased relative density of mechanoreceptors in the distal paw suggests that this area serves as a tactile fovea and coincides with fine-scale observations of sea otter behavior during object exploration and manipulation. Combined with previous measurements of sea otter touch abilities using psychophysical methods, the results from this study support the general conclusion that sea otter paws have derived features and function as sensitive receptors that can efficiently detect and capture visually cryptic prey, as well as dexterously handle tools and captured prey.

ACKNOWLEDGMENTS

We thank Laird Henkel, Francesca Batac, Erin Dodd, Colleen Young, and Angie Reed at California Department of Fish and Wildlife's Marine Wildlife Veterinary Care and Research Center, who first brought our attention to Pacinian corpuscles in sea otter skin and provided facilities and resources for sample preparation. We thank Andy Johnson, Erin Lenihan, and Marissa Young at Monterey Bay Aquarium for sample collection and Lilian Carswell at US Fish and Wildlife Service for assistance

with federal authorizations for this research. Many individuals provided advice and offered expertise throughout the development of this project, including Alan Shabel, Alex Ehrenberg, and Shawn Shirazi at the University of California Berkeley; Verena Affolter, Becky Griffey, and Amber Villarreal at the Veterinary Histology Lab at the University of California Davis, Richard Luong at IDEXX, and Frank Rice at Integrated Tissue Dynamics. Ben Abrams at the Microscopy Center at the University of California Santa Cruz was an invaluable source of microscopy support, and Tom Yuzvinsky at the W.M. Keck Center for Nanoscale Optofluidics at the University of California Santa Cruz performed the scanning electron microscopy. Juliette Linossier and Sarah Santich assisted with time-sensitive histological sample preparation. Tim Tinker, Pete Raimondi, Bruce Lyon, James Estes, and Rita Mehta in the Ecology and Evolutionary Biology Department at the University of California Santa Cruz contributed to the interpretation of this research. Portions of this manuscript were included in the doctoral dissertation of Sarah McKay Strobel submitted to the University of California Santa Cruz in August 2019. Sarah McKay Strobel was supported by the Department of Education Graduate Assistance in Areas of National Need Fellowship P200A150100. Direct research costs were supported by the Sea Otter Foundation and Trust.

CONFLICT OF INTEREST

The authors declare no potential conflict of interest.

AUTHOR CONTRIBUTIONS

Sarah McKay Strobel: Conceptualization (lead); data curation (lead); formal analysis (lead); funding acquisition (lead); investigation (lead); methodology (lead); project administration (lead); resources (supporting); software (lead); supervision (equal); validation (equal); visualization (lead); writing-original draft (lead). **Melissa Miller:** Resources (supporting); supervision (supporting); validation (supporting); writing-review & editing (supporting). **Michael Murray:** Resources (supporting); writing-review & editing (supporting). **Colleen Reichmuth:** Conceptualization (supporting); funding acquisition (supporting); project administration (supporting); resources (equal); supervision (equal); validation (equal); visualization (supporting); writing-original draft (supporting); writing-review & editing (supporting).

DATA AVAILABILITY STATEMENT

We plan to publish the histological and SEM images used for quantitative and qualitative evaluation of mechanoreceptors and skin texture at Dryad. Any other data related to the findings of this study are available from the

corresponding author, Sarah McKay Strobel, upon reasonable request.

ETHICS STATEMENT

All procedures were in accordance with the ethical standards of the University of California Santa Cruz and with federal regulations of the United States. Postmortem samples were collected and processed under Letters of Authorization from the US Fish and Wildlife Service (08EVEN00-2016-B-0187 and 08EVEN00-2017-B-0045) with the approval and oversight of the Institutional Animal Care and Use Committee at the University of California Santa Cruz and the Research Oversight Committee at Monterey Bay Aquarium. This article does not contain studies of human participants.

ORCID

Sarah McKay Strobel  <https://orcid.org/0000-0002-5259-0589>

Colleen Reichmuth  <https://orcid.org/0000-0003-0981-6842>

REFERENCES

- Abrahams, V. C., Hodgins, M., & Downey, D. (1987). Morphology, distribution, and density of sensory receptors in the glabrous skin of the cat rhinarium. *Journal of Morphology*, *191*, 109–114.
- Adams, T., & Hunter, W. S. (1969). Modification of skin mechanical by eccrine sweat gland activity properties. *Journal of Applied Physiology*, *26*(4), 417–419.
- Adelman, S., Taylor, C. R., & Heglund, N. C. (1975). Sweating on paws and palms: What is its function? *The American Journal of Physiology*, *229*(5), 1400–1402.
- Andres, K. H., & v Düring, M. (1990). Comparative and functional aspects of the histological organization of cutaneous receptors in vertebrates. In W. Zenker & W. L. Neuhuber (Eds.), *The primary afferent neuron: A survey of recent morpho-functional aspects* (pp. 1–17). New York, NY: Plenum Press.
- Bates, D., Maechler, M., Bolker, B., & Walker, S. (2015). Fitting linear mixed-effects models using lme4. *Journal of Statistical Software*, *67*, 1–48.
- Bell, J., Bolanowski, S., & Holmes, M. H. (1994). The structure and function of Pacinian corpuscles: A review. *Progress in Neurobiology*, *42*, 79–128.
- Bodkin, J. L., Esslinger, G. G., & Monson, D. H. (2004). Foraging depths of sea otters and implications to coastal marine communities. *Marine Mammal Science*, *20*, 305–321.
- Bolanowski, S. J., & Pawson, L. (2003). Organization of Meissner corpuscles in the glabrous skin of monkey and cat. *Somatosensory & Motor Research*, *20*, 223–231.
- Bolanowski, S. J., & Verrillo, R. T. (1982). Temperature and criterion effects in a somatosensory subsystem: A neurophysiological and psychophysical study. *Journal of Neurophysiology*, *48*, 836–855.
- Bouley, D. M., Alarcón, C. N., Hildebrandt, T., & O'Connell-Rodwell, C. E. (2007). The distribution, density and three-dimensional histomorphology of Pacinian corpuscles in the foot

- of the Asian elephant (*Elephas maximus*) and their potential role in seismic communication. *Journal of Anatomy*, 211, 428–435.
- Brenowitz, G. L. (1980). Cutaneous mechanoreceptor distribution and its relationship to behavioral specializations in squirrels. *Brain, Behavior and Evolution*, 17, 432–453.
- Bruce, M. (1980). The relation of tactile thresholds to histology in the fingers of elderly people. *Journal of Neurology, Neurosurgery, and Psychiatry*, 43, 730–734.
- Cartmill, M. (1979). The volar skin of primates: Its frictional characteristics and their functional significance. *American Journal of Physical Anthropology*, 50, 497–510.
- Cauna, N. (1985). Nature and functions of the papillary ridges of the digital skin. *The Anatomical Record*, 119(4), 449–468.
- Chinn, S. M., Miller, M. A., Tinker, M. T., Staedler, M. M., Batac, F. I., Dodd, E. M., & Henkel, L. A. (2016). The high cost of motherhood: End-lactation syndrome in southern sea otters (*Enhydra lutris nereis*) on the Central California coast, USA. *Journal of Wildlife Diseases*, 52, 307–318.
- Costa, D. P., & Kooyman, G. L. (1982). Oxygen consumption, thermoregulation, and the effect of fur oiling and washing on the sea otter, *Enhydra lutris*. *Canadian Journal of Zoology*, 60, 2761–2767.
- da Silva, A. P., Machado, A. S. D., Le Bas, A. E., Silva, R. G., dos Anjos Silva, E., & Hernandez-Blazquez, F. J. (2020). The skin structures and their role in the thermoregulation of the South American fur seal (*Arctocephalus australis*). *The Anatomical Record*, 303, 3155–3167.
- Estes, J. A., Hatfield, B. B., Ralls, K., & Ames, J. (2003). Causes of mortality in California sea otters during periods of population growth and decline. *Marine Mammal Science*, 19(1), 198–216.
- Fay, F. H. (1982). *Ecology and biology of the Pacific walrus, Odobenus rosmarus divergens*. Washington, DC: U.S. Fish and Wildlife Service.
- Fujii, J. A., Ralls, K., & Tinker, M. T. (2015). Ecological drivers of variation in tool-use frequency across sea otter populations. *Behavioral Ecology*, 26, 519–526.
- Gescheider, G. A., Thorpe, J. M., Goodarz, J., & Bolanowski, S. J. (1997). The effects of skin temperature on the detection and discrimination of tactile stimulation. *Somatosensory & Motor Research*, 14, 181–188.
- Gonzalez-Martinez, T., Germana, G. P., Monjil, D. F., Silos-Santiago, I., de Carlos, F., Germana, G., ... Vega, J. A. (2004). Absence of Meissner corpuscles in the digital pads of mice lacking functional TrkB. *Brain Research*, 1002(1-2), 120–128.
- Halata, Z. (1990). Sensory innervation of the hairless and hairy skin in mammals including humans. In W. Zenker & W. L. Neuhuber (Eds.), *The primary afferent neuron: A survey of recent morpho-functional aspects* (pp. 19–34). New York, NY: Plenum Press.
- Halata, Z., & Munger, B. L. (1983). The sensory innervation of primate facial skin. II. Vermilion border and mucosa of lip. *Brain Research Review*, 5, 81–107.
- Hall, K. R. L., & Schaller, G. B. (1964). Tool-using behavior of the California Sea otter. *Journal of Mammalogy*, 45, 287–298.
- Hamrick, M. W. (2001). Morphological diversity in digital skin microstructure of didelphid marsupials. *Journal of Anatomy*, 198, 683–688.
- Hochberg, Y. (1988). A sharper Bonferroni procedure for multiple tests of significance. *Biometrika*, 75(4), 800–802.
- Hoffmann, J. N., Montag, A. G., & Dominy, N. J. (2004). Meissner corpuscles and somatosensory acuity: The prehensile appendages of primates and elephants. *Anatomical Record Part A: Discoveries in Molecular, Cellular, and Evolutionary Biology*, 281, 1138–1147.
- Hothorn, T., Bretz, F., & Westfall, P. (2008). Simultaneous inference in general parametric models. *Biometrical Journal*, 50, 346–363.
- Ide, C. (1977). Development of Meissner corpuscle of mouse toe pad. *The Anatomical Record*, 188(1), 49–67.
- Iggo, A., & Andres, K. H. (1982). Morphology of cutaneous receptors. *Annual Review of Neuroscience (Palo Alto, CA)*, 5, 1–31.
- Iggo, A., & Muir, A. R. (1969). The structure and function of a slowly adapting touch corpuscle in hairy skin. *Journal of Physiology*, 200, 763–796.
- Johansson, R. S., & Vallbo, A. B. (1979). Tactile sensibility in the human hand: Relative and absolute densities of four types of mechanoreceptive units in glabrous skin. *The Journal of Physiology*, 286, 283–300.
- Johnson, K. O. (2001). The roles and functions of cutaneous mechanoreceptors. *Current Opinion in Neurobiology*, 11, 455–461.
- Johnson, K. O., & Hsiao, S. S. (1992). Neural mechanisms of tactual form and texture perception. *Annual Review of Neuroscience*, 15, 227–250.
- Kellogg, D. L. (2006). In vivo mechanisms of cutaneous vasodilation and vasoconstriction in humans during thermoregulatory challenges. *Journal of Applied Physiology*, 100, 1709–1718.
- Kenyon, K. (1969). *The sea otter in the eastern Pacific Ocean*. North American Fauna, 68, Washington, DC, USA: Bureau of Sport Fisheries and Wildlife.
- Klatzky, R. L., & Lederman, S. J. (2003). Touch. In A. F. Healy, R. W. Proctor & I. B. Weiner (Eds.), *Experimental Psychology, Handbook of Psychology* (vol. 4, pp. 147–176). New York, NY: Wiley.
- Kreuder, C., Miller, M. A., Jessup, D. A., Lowenstine, L. J., Harris, M. D., Ames, J. A., ... Mazet, J. A. K. (2003). Patterns of mortality in southern sea otters (*Enhydra lutris nereis*) from 1998–2001. *Journal of Wildlife Diseases*, 39, 495–509.
- Kuhn, R. A., Ansorge, H., Godynicki, S., & Meyer, W. (2010). Hair density in the Eurasian otter *Lutra lutra* and the sea otter *Enhydra lutris*. *Acta Theriologica (Warsz.)*, 55, 211–222.
- Kumamoto, K., Senuma, H., Ebara, S., & Matsuura, T. (1993). Distribution of Pacinian corpuscles in the hand of the monkey, *Macaca fuscata*. *Journal of Anatomy*, 183, 149–154.
- Kumamoto, K., Takei, M., Kinoshita, M., Ebara, S., & Matsuura, T. (1993). Distribution of Pacinian corpuscles in the cat forefoot. *Journal of Anatomy*, 182, 23–28.
- Lacour, J. P., Dubois, D., Pisani, A., & Ortonne, J. P. (1991). Anatomical mapping of Merkel cells in normal human adult epidermis. *The British Journal of Dermatology*, 125, 535–542.
- Ling, J. K. (2018). A histological study of the skin, hair follicles and moult of the hooded seal (*Cystophora cristata* [Erxleben, 1777]). *Polar Research*, 37, 1419906.
- Merkel, F. (1875). Tastzellen und Tastkörperchen bei den Hausthieren und beim Menschen. *Archiv für mikroskopische Anatomie*, 11, 636–654.
- Meyer, W., Bartels, T. I., Tsukise, A., & Neurand, K. (1990). Histochemical aspects of stratum corneum function in the feline foot pad. *Archives of Dermatological Research*, 281, 541–543.

- Meyer, W., & Tsukise, A. (1995). Lectin histochemistry of snout skin and foot pads in the wolf and domesticated dog (Mammalia: Canidae). *Annals of Anatomy*, 177(1), 39–49.
- Montagna, W., Roman, N. A., & Macpherson, E. (1975). Comparative study of the innervation of the facial disc of selected mammals. *The Journal of Investigative Dermatology*, 65(5), 458–465.
- Munger, B. L., & Halata, Z. (1983). The sensory innervation of primate facial skin. I. Hairy skin. *Brain Research Review*, 5, 45–80.
- Munger, B. L., & Ide, C. (1988). The structure of cutaneous sensory receptors. *Archives of Histology and Cytology*, 51(1), 1–34.
- Munger, B. L., & Pubols, L. M. (1972). The sensorineural organization of the digital skin of the raccoon. *Brain, Behavior and Evolution*, 5, 367–393.
- Mykytowycz, R. (1972). The behavioural role of the mammalian skin glands. *Naturwissenschaften*, 59, 133–139.
- Nava, P. B., & Mathewson, R. C. (1996). Effect of age on the structure of Meissner corpuscles in murine digital pads. *Microscopy Research and Technique*, 34, 376–389.
- Paré, M., Smith, A. M., & Rice, F. L. (2002). Distribution and terminal arborizations of cutaneous mechanoreceptors in the glabrous finger pads of the monkey. *The Journal of Comparative Neurology*, 445, 347–359.
- Pocock, R. I. (1928). Some external characters of the sea-otter (*Enhydra lutris*). *Proceedings of the Zoological Society of London*, 98(4), 983–991.
- Radinsky, L. B. (1968). Evolution of somatic sensory specialization in otter brains. *The Journal of Comparative Neurology*, 134, 495–506.
- Rasmussen, L. E. L., & Munger, B. L. (1996). The sensorineural specializations of the trunk tip (finger) of the Asian elephant, *Elephas maximus*. *The Anatomical Record*, 246, 127–134.
- Rice, F. L., & Rasmusson, D. D. (2000). Innervation of the digit on the forepaw of the raccoon. *The Journal of Comparative Neurology*, 417, 467–490.
- Riedman, M. L., & Estes, J. A. (1990). The sea otter *Enhydra lutris*: Behavior, ecology, and natural history. *Biology Reports—U.S. Fish and Wildlife Service*, 90, 1–136.
- Rothman, S., & Lorincz, A. L. (1963). Defense mechanisms of the skin. *Annual Review of Medicine*, 14, 215–242.
- Schindelin, J., Arganda-Carreras, I., Frise, E., Kaynig, V., Longair, M., Pietzsch, T., ... Cardona, A. (2012). Fiji: An open-source platform for biological-image analysis. *Nature Methods*, 9, 676–682.
- Silverman, R. T., Munger, B. L., & Halata, Z. (1986). The sensory innervation of the rat rhinarium. *The Anatomical Record*, 214(2), 210–225.
- Sokolov, V. E. (1982). Comparative morphology of skin of different orders. In *Mammal skin* (pp. 43–572). Berkeley, CA: University of California Press.
- Staedler, M., & Riedman, M. (1993). Fatal mating injuries in female sea otters (*Enhydra lutris nereis*). *Mammalia*, 57, 135–139.
- Stark, B., Carlstedt, T., Hallin, R. G., & Risling, M. (1998). Distribution of human Pacinian corpuscles in the hand: A cadaver study. *Journal of Hand Surgery (European Volume)*, 23(3), 370–372.
- Strobel, S. M., Sills, J. M., Tinker, M. T., & Reichmuth, C. J. (2018). Active touch in sea otters: In-air and underwater texture discrimination thresholds and behavioral strategies for paws and vibrissae. *Journal of Experimental Biology*, 221, jeb181347.
- Stumpf, P., Künzle, H., & Welsch, U. (2004). Cutaneous eccrine glands of the foot pads of the small Madagascan tenrec (*Echinops telfairi*, Insectivora, Tenrecidae): Skin glands in a primitive mammal. *Cell and Tissue Research*, 315, 59–70.
- Tachibana, T., & Fujiwara, N. (1991). Mechanoreceptors of the hard palate of the mongolian gerbil include special junctions between epithelia and Meissner lamellar cells: A comparison with other rodents. *The Anatomical Record*, 231, 396–403.
- Venkatesan, L., Barlow, S. M., & Kieweg, D. (2015). Age- and sex-related changes in vibrotactile sensitivity of hand and face in neurotypical adults. *Somatosensory & Motor Research*, 32, 44–50.
- Verendeev, A., Thomas, C., McFarlin, S. C., Hopkins, W. D., Phillips, K. A., & Sherwood, C. C. (2015). Comparative analysis of Meissner's corpuscles in the fingertips of primates. *Journal of Anatomy*, 227, 72–80.
- Verrillo, R. T., & Bolanowski, S. J. (1986). The effects of skin temperature on the psychophysical responses to vibration on glabrous and hairy skin. *The Journal of the Acoustical Society of America*, 80, 528–532.
- Weissengruber, G. E., Egger, G. F., Hutchinson, J. R., Groenewald, H. B., Elsässer, L., Famini, D., & Forstenpointner, G. (2006). The structure of the cushions in the feet of African elephants (*Loxodonta africana*). *Journal of Anatomy*, 209, 781–792.
- Wickremaratchi, M. M., & Llewelyn, J. G. (2006). Effects of ageing on touch. *Postgraduate Medical Journal*, 82(967), 301–304.
- Williams, T. D., Allen, D. D., Groff, J. M., & Glass, R. L. (1992). An analysis of California Sea otter (*Enhydra lutris*) pelage and integument. *Marine Mammal Science*, 8, 1–18.
- Winkelmann, R. K. (1964). Nerve endings of the north American opossum (*Didelphis virginia*): A comparison with nerve endings of primates. *American Journal of Physical Anthropology*, 22(3), 253–258.
- Yeates, L. C., Williams, T. M., & Fink, T. L. (2007). Diving and foraging energetics of the smallest marine mammal, the sea otter (*Enhydra lutris*). *The Journal of Experimental Biology*, 210, 1960–1970.
- Young, B., O'Dowd, G., & Woodford, P. (2014). *Wheater's functional histology: A text and colour atlas* (6th ed.). Philadelphia, PA: Elsevier Churchill Livingstone.

SUPPORTING INFORMATION

Additional supporting information may be found in the online version of the article at the publisher's website.

How to cite this article: Strobel, S. M., Miller, M. A., Murray, M. J., & Reichmuth, C. (2021). Anatomy of the sense of touch in sea otters: Cutaneous mechanoreceptors and structural features of glabrous skin. *The Anatomical Record*, 1–21. <https://doi.org/10.1002/ar.24739>